Activated char from the co-pyrolysis of polystyrene and olive stone mixtures for the adsorption of CO_2

Rafael R. Solís*, Mª Carmen González, Gabriel Blázquez, Mónica Calero*, Mª Ángeles Martín-Lara

Department of Chemical Engineering, University of Granada, 18074 Granada, Spain

*Correspondence to Rafael R. Solís (rafarsolis@ugr.es) and Mónica Calero (mcaleroh@ugr.es)

Abstract

Yogurt plastic containers made of polystyrene (PS), olive stone, and mixtures of both have been converted into activated carbon materials transforming them firstly into char via pyrolysis and secondly with activation of either KOH or H_2SO_4. The pyrolysis of the olive stone gave a higher yield of material than the plastic PS. However, the activation of the PS char with KOH was more effective, reaching surface areas of 508 vs 194 $m^2 g^{-1}$ of the corresponding prepared with olive stone. The prepared materials were tested as CO_2 adsorbent in thermobalance and fixed-be column assays. The materials activated with H_2SO_4 slightly enhanced the adsorption ability of the original char but were far from the performance obtained with KOH activation. The CO_2 isotherms showed high synergy of CO_2 uptake and selectivity when using activated chars prepared with the char from the mixture of raw materials, specially at a 1:1 ratio. The isosteric heat of adsorption values were the expected for a physisorption process. Further experiments in a fixed-bed column were also studied at atmospheric pressure at different inlet CO_2 concentrations (10-50%). The CO_2 retention increased as the partial CO_2 pressure rose. Besides, a very similar performance of the material prepared with plastic and olive stones was obtained at 50%, i.e. 220 and 197 mg g^{-1} respectively. At low CO_2 concentrations, the materials enriched with plastic displayed better performance than those prepared with olive stone. Cycles of adsorption-desorption were carried out in the

column to assess the stability of the materials. The curves obtained did not display any substantial change, demonstrating the lack of adsorption retention.

Keywords: pyrolysis; char; polystyrene; olive stones; activation; CO_2 adsorption

1. INTRODUCTION

The discovery and industrial manufacturing of plastic have posed a great development since they were mass-produced in the 1950s due to their versatile properties. Their use is ubiquitous in almost all economic sectors. Plastic consumption has vertiginously risen. By 2050, it is expected to have produced 1000 million tons of plastics [1]. Currently, on average, only 9% of the released plastics are recycled [2]. The rest is landfilled or polluting the natural ecosystems. The alarming presence of plastics in the environment is stressing and challenging the natural life development of living organisms [3]. The presence of micro-sized plastics has been widespread all over the World with a special impact on marine fauna [4,5].

Packaging is the sector that consumes the largest plastics amount and also the sector with the shortest life [6]. After use, the plastics used for packaging are discharged. Those that are easily recycled mechanically are incorporated in the plastic circle manufacture, promoting therefore the circular economy. However, the complexity in terms of composition and complex management makes little applicability the mechanical recycling, especially in the rejected fractions from urban wastes. In this case, recycling through chemical strategies represents a more competitive alternative. Chemical recycling consists of the breakage of the polymer into monomers by chemical [7], biological [8] enzymatic reactions [9], or pyrolysis [10,11].

The pyrolysis or the thermal lysis of the polymeric chains allows to obtain three fractions [12]: a gas generally enriched in methane and other incondensable hydrocarbons up to butane; a liquid or oil fraction of variable composition depending on the starting polymer; and a solid residue. The solid waste obtained, namely char, is rich in carbon and the production yield depends on the operating conditions during the pyrolysis process [13]. Thus, low heating rates, low temperature, and long residence

55 times have been found to maximize the char yield. The gas and the oil released have
56 potential applications as fuels; however, the char is considered a residue with little
57 further interest due to the low yield it produces. Some applications under research are
58 the construction of asphalts [14], fuel briquettes [15], the use as an additive in epoxy
59 resins [16,17], or as adsorbent after activation for environmental applications such as
60 the removal of pollutants in aqueous effluents [18–20] of gas purification such as the
61 CO_2 capture [21–23].

62 This work studies the preparation of porous activated carbon obtained from mixed
63 wastes, yogurt containers made of polystyrene (PS), and olive stone. The individual
64 materials and mixed fractions have been subjected to pyrolysis and the char obtained
65 was further activated chemically with KOH and H_2SO_4. The textural properties were
66 characterized before and after activation, registering great effectiveness when KOH was
67 used. The resulting material was used as an adsorbent for the removal of CO_2 in the gas
68 phase at 30 ºC and atmospheric pressure, which simulated the conditions of combustion
69 gases. The CO_2 uptake was quantified in thermobalance assays. The materials with the
70 best CO_2 uptake in thermobalance assays after activation were further considered for
71 analysis in the fixed-bed column. The influence of the inlet CO_2 concentration was
72 investigated within 10 to 50%.

73 **2. EXPERIMENTAL SECTION**

74 **2.1. Preparation and activation of the co-pyrolysis chars**

75 High-impact polystyrene (HIPS) was obtained from yogurt containers. After
76 removing the labeling, the plastic packages were washed, dried, and crushed to less than
77 1 mm. The olive stones were acquired from a local olive oil mill supplier in Granada
78 (Spain). The stones were dried and crushed to less than 1 mm in size.

79 The co-pyrolysis of the HIPS and olive stones was carried out in a furnace under an
80 N_2 atmosphere by mixing the crushed starting materials. Around 20 g of material was
81 placed in a tubular metallic container. Different mixtures of plastic and olive stones
82 were pyrolyzed, i.e. 80% plastic (80P), 50% plastic (50P), and 20% plastic (20P). The
83 chars from pure plastic (P-char) or olive stone (OS-char) were also prepared. The
84 samples were heated under an N_2 flow rate of 50 L h^{-1} from room temperature to 500 ºC
85 (heating rate 10 ºC min^{-1}). Next, the temperature was kept at 500 ºC for 90 min and
86 finally cooled down naturally under an N_2 atmosphere. The char yield in each case is
87 shown in **Table 1**.

88 **Table 1.** Char yield during the pyrolysis of polystyrene-olive stone mixtures

Starting mixture	Yield (%)
Plastic	10.6
80% Plastic	14.6
50% Plastic	20.2
20% Plastic	25.9
Olive stone	28.5

89 The resulting chars were activated chemically with KOH and H_2SO_4. The selection
90 of the activation temperature and KOH-char ratio was based on preliminary studies and
91 environmental concerns. Initial tests (results not shown) pointed out that P-char
92 displayed an optimum activation temperature of 800 ºC, whereas the OS-char displayed
93 a positive effect on the porosity up to 850 ºC. Based on that premise, and the
94 environmental cost of the energy required for the activation process, 800 ºC was
95 selected for this study. Pertaining to the KOH proportion, a previous study of activation
96 of a char prepared from a mixture of plastics showed that a mass ratio of 1:1 for KOH
97 was optimum for developing the highest microporosity [24]. Since the optimization of
98 the KOH-ratio is out of the scope of this work and a higher proportion would negatively
99 impact the environmental cost of the final material, a mass ratio 1:1 was selected. The

activation of KOH was conducted with 2.5 g of char and 2.5 g of KOH, mixed, and placed in the metallic capsule of the furnace. Under the N_2 atmosphere (200 mL min^{-1}), the temperature was raised from 10 ºC min^{-1} to 300 ºC and kept at this temperature for 1 hour to melt the KOH. Next, under the same heating rate, the temperature was raised to 800 ºC and kept for 1 h. After cooling to room temperature under an N_2 atmosphere, the resulting sample was washed several times with HCl 1 M and water and finally dried at 120 ºC for 24 h. For the activation with H_2SO_4, 2.5 g of char was suspended in 25 mL of H_2SO_4 at 20%. The suspension was stirred and then dried at 110 ºC. After, the sample was heated under an N_2 atmosphere (200 mL min^{-1}) to 300 ºC (10 ºC min^{-1}) and held for 1 h. For comparison purposes, the non-activated chars were also washed with HCl 1 M and water and dried at 120 ºC for 24 h.

2.2. Characterization of the activated chars

The textural and surface properties were assessed by N_2 adsorption-desorption isotherms at -196 ºC in a Sync 200 device of 3P Instruments©. Firstly, the samples were degassed at 150 ºC for 12 h in a Prep J4 unit of 3P Instruments© under vacuum. The Brunauer-Emmett-Teller (BET) method was used for the determination of the total specific surface area (S_{BET}). The total pore volume (V_T) was quantified from the N_2 uptake at $p/p_0 \sim 0.99$. The t-plot method was applied to determine the specific surface of micropores (S_{MP}) and the volume of micropores (V_{MP}). The micropore size distribution was studied using CO_2 adsorption isotherms at 0 ºC applying the Horvath–Kawazoe (HK) method [25,26].

The disorder degree of carbon was studied by X-ray Diffraction (XRD) in a Bruker D8 Discover device equipped with a detector Pilatus3R 100K-A, working with Cu Kα radiation (λ = 1.5406 Å). The diffractograms were registered within the 2θ range of 5–75°.

125 The presence of surface functional groups was analyzed by attenuated total
126 reflectance Fourier transform Infrared (ATR-FTIR) in a Perkin-Elmer Spectrum 65
127 device, registering the spectra within 4000 and 400 cm^{-1} (resolution of 2 cm^{-1}).

128 The elemental analysis was carried out in a CHNS/O analyzer, model Flash 2000
129 from Thermo Scientific^{TM}. Briefly, the sample was oxidized at approximately 1400 °C
130 and the released gases (CO_2, H_2O, NO_x, SO_x, and unreacted O_2) passed through to the
131 capture of O_2 (copper bed at 860 °C) and led to the reduction of the organic nitrogen
132 and sulfur to N_2 and SO_2. The final gases (CO_2, H_2O, N_2, and SO_2) are separated by gas
133 chromatography and the quantification is conducted by thermal conductivity detection.
134 The amount of oxygen is determined by the difference.

135 The morphology of the porous activated samples was analyzed by Scanning Electron
136 Microscopy (SEM) in a FEI Quanta 400 device (30 kV, 3.5 nm resolution).
137 Transmission Electron Microscopy (TEM) was also conducted in a Libra LIBRA 120
138 PLUS from Carl Zeiss SMT (120 kV, LaB_6 filament), equipped with an omega in-line
139 filter and Electron Energy Loss Spectroscopy (EELS) detection, which was conducted
140 as a complementary analysis to assess the disorder degree of carbon, i.e. graphitic or
141 amorphous carbon.

142 **2.3. Adsorption of CO_2: kinetics and thermodynamics**

143 The CO_2 isotherms at 0 and 25 ºC were carried out in a Sync 200 device of 3P
144 Instruments©. The samples were degassed as mentioned previously. The CO_2 uptake
145 (q_{CO2}, mg g^{-1}) was adjusted to the Freundlich equation [27]:

146 $$q_{CO_2} = K_F \, p^{1/n_F} \quad (1)$$

147 where K_F (mg g^{-1} kPa^{-nF}) and n_F are, respectively, the Freundlich constant and exponent.

148 The CO_2/N_2 selectivity was calculated from their respective isotherms conducted at
149 25ºC, near ambient temperatures that are relevant for real applications. The selectivity
150 of CO_2/N_2 was estimated using the Henry's law, by dividing the initial slopes of CO_2
151 and N_2 adsorption isotherms [28], obtained by adjusting the isotherm data to a straight
152 line within 0-20 kPa. Alternatively, the selectivity as a function of the total pressure was
153 determined considering the ideal adsorbed solution theory (IAST), based on the
154 assumption of a typical fuel gas composition, i.e., 15:85 (v/v) CO_2:N_2. Hence, the
155 selectivity was calculated as follows [29,30]:

156 $$\text{Selectivity} = \left(\frac{V_{CO_2,25^\circ C}}{V_{N_2,25^\circ C}}\right)\left(\frac{p_{N_2}}{P_{CO_2}}\right) \quad (2)$$

157 where V_i stands for the gas uptake (STP $cm^3\ g^{-1}$) and p_i is the partial pressure of the i
158 component in the CO_2-N_2 mixture (p_{N2}/p_{CO2}=0.85/0.15).

159 The isosteric heat of adsorption (ΔH_{ads}) was obtained as a function of the CO_2 uptake
160 (q_{CO2}) with the Clausius–Clapeyron equation [31,32]:

161 $$\Delta H_{ads} = -R \ln\left(\frac{P_2}{P_1}\right)\frac{T_1 T_2}{(T_2 - T_1)} \quad (3)$$

162 The obtained parameters by the Freundlich model were applied to the two adsorption
163 isotherms carried out at T_1=0 ºC and T_2=25 ºC to obtain the pressures (p_1 and p_2) for
164 different CO_2 adsorption uptakes, leading to the isosteric adsorption calculation.

165 The adsorption capacity (q_{CO2}) was quantified by thermogravimetric assays in a
166 Perkin-Elmer STA 6000 thermobalance. The process was set up with a drying step for
167 the removal of moisture and physisorbed substances. The sample (10-20 mg) was
168 subjected to a heating step from room temperature to 200 ºC and then held to this value
169 for 1 h, under an N_2 atmosphere, flow rate of 50 mL min^{-1}. Next, the sample was cooled
170 to 30 ºC under the same N_2 flow rate. Finally, the isothermal adsorption step of CO_2 was

done by changing the inlet gas to CO_2, 50 mL min^{-1}, for 2 h, until a constant mass was observed. The increase of mass registered for the mass of the dried sample led to the determination of the adsorbed CO_2.

Two models were used to describe the kinetic adsorption process of CO_2 onto the carbonaceous adsorbents, i.e. pseudo-first-order and Avrami models, previously applied to simulate the adsorption rate behavior in similar materials [33–35]. The Lagergren's pseudo-first order model assumes that the rate of CO_2 depletion is directly proportional to the difference between the saturation concentration of that species and the mean concentration within the particle [36], describing the temporal evolution of the adsorbed CO_2 capacity as follows:

$$q_{CO_2} = q_S\left(1 - e^{-k_1 t}\right) \quad (4)$$

where q_S (mg g^{-1}) is the CO_2 adsorption capacity under saturation conditions and k_1 (min^{-1}) is the pseudo-first order rate constant. The Avrami model is a three-parameter modification of the first-order kinetics that was originally developed to simulate the phase transitions and crystal growth of materials [37]. Recently, it has been successfully used to describe the kinetics of CO_2 adsorption onto functionalized activated carbons [33,38], clays [35] and zeolites [39]. The model predicts the evolution of the adsorbed CO_2 as follows:

$$q_{CO_2} = q_S\left(1 - e^{-(k_A t)^{n_A}}\right) \quad (5)$$

where k_A (min^{-1}) is the Avrami kinetic constant and n_A (dimensionless) is the Avrami exponent.

2.4. Breakthrough curves of CO_2 adsorption in a fixed-bed column

The breakthrough curves of CO_2 adsorption in fixed-bed assays were carried out in a jacket glass column of 10 cm length and 10 mm internal diameter. The temperature was set at 30 ºC with the use of a cooling fluid passing through the annular space of the column. In the inlet, 0.5 g of adsorbent was placed. Glass balls were placed in the extremes of the adsorbent to keep it immobilized and avoid fluidization. A gas flow rate of N_2-CO_2 mixtures (C_0=10-30% of CO_2) at a total flow rate of 100 mL min^{-1} was fed to the bottom of the column. The concentration of CO_2 leaving the column was analyzed by infrared detection (NDIR Edinburgh Instruments Ltd.). For the adsorption-desorption cycles, after reaching saturation of CO_2 adsorption, the mixture N_2-CO_2 was changed into pure N_2 to complete the desorption step.

The adsorption capacity of CO_2 (q_{CO2}) was quantified from the area below the removed CO_2 curve from the beginning of the process until reaching saturation of the column (t_{sat}), i.e. C/C_0~0.95, as follows:

$$q_{CO_2} = \frac{\vartheta C_0}{m_{ads}} \int_0^{t_{sat}} \left(1 - \frac{C}{C_0}\right) dt \quad (6)$$

where υ (L s^{-1}) means the volumetric flow rate, C_0 (mol L^{-1}) is the inlet CO_2 concentration, and m_{Ads} is the mass of the adsorbent loaded in the column.

The removal efficiency of CO_2 was determined as the amount of CO_2 adsorbed in the fixed-bed respect to the total fed in the column:

$$R = \frac{q_{CO_2} m_{ads}}{\vartheta C_0 t_{sat}} = \frac{\int_0^{t_{sat}} \left(1 - \frac{C}{C_0}\right) dt}{t_{sat}} \quad (7)$$

3. RESULTS AND DISCUSSION

3.1. Characterization of the materials

The textural properties of the materials after chemical activation with KOH and H_2SO_4 were evaluated by N_2 adsorption-desorption isotherms at -196 ºC, see results in **Figure 1** and **Table 2**. As can be seen, the activation with KOH led to the best results. The char prepared from polystyrene after KOH activation led to a higher surface area (508 vs 194 $m^2\ g^{-1}$) and pore volume (0.398 vs 0.116 $m^2\ g^{-1}$) than the activation of the char obtained from olive stone. Their relative mixtures led to intermediate values except for the sample 80P-char-KOH which led to a higher surface area, i.e. 559 $m^2\ g^{-1}$. The isotherms describe a type II shape according to the IUPAC's classification [40], with a high increase of N_2 uptake at low relative pressures, which means a good development of microporosity. Plastic displayed higher micropore volume than olive stone. However, in relative terms, the presence of olive stone, although decreases the global porosity reached in the final material, affects positively the microporosity ratio (see **Table 2**). The higher contribution when plastic is incorporated is also deduced from the H4-type hysteresis loop [41].

Although the pyrolysis of plastic residues has been extensively studied for the production of added-value fuels, there is less information in the literature about the use of char using high-impact polystyrene as the precursor for the production of activated carbon materials [22]. Expanded polystyrene foams have led to very porous structures, over 2000 $m^2\ g^{-1}$ surface area, and ~1 $cm^3\ g^{-1}$ of pore volume [42]. The pyrolysis of waste tires and their activation with KOH has been reported to produce activated carbon with 474 $m^2\ g^{-1}$ (700 ºC, KOH amount 4 times folded to the char) [43]. The acid activation with H_3PO_4 has been reported to develop much less porosity, 37-74 $m^2\ g^{-1}$ depending on the temperature of the process. Other studies have reached improved

237 textural, with areas as high as 700 m^2 g^{-1} from activating the waste tires with a higher
238 KOH ratio, i.e. five [44] or six times higher than the char [19]. A rise of the activating
239 agent, although develops higher porosity, implies a rise in the costs of the material by
240 the use of more chemical agents and further washing efforts. Bottles of polyethylene
241 terephthalate have been pyrolyzed and the resulting char after activation with KOH
242 (ratio KOH: char 3:1) led to a porous carbon material of high specific surface area
243 (1345 m^2 g^{-1}) [45]. The char obtained from non-recyclable mixtures of plastic wastes
244 after activation with KOH has led to surface areas of 487 m^2 g^{-1} [46].

245 The pyrolysis and activation conditions have been selected based on the behavior of
246 the plastic [24]. Nonetheless, the activation of olive stones has been widely studied in
247 the literature, and optimized to release very porous carbon materials. The activation of
248 olive stones with KOH under similar activation conditions (800 ºC, KOH: olive stone
249 1:1) has been reported to develop porosity as high as 500 m^2 g^{-1}, and even higher by
250 raising the ratio of KOH to the char [47]. Other works have reported higher BET area
251 values with KOH activation, such as 886 mg^2 g^{-1} at optimal conditions for the activation
252 at 715 ºC, 2 hours, an amount 1.5 times KOH to char [48]. Besides, the carbonization
253 temperature of the olive stones at lower temperatures, i.e. 200 ºC, and further activation
254 with a high ratio of KOH, i.e. 3:1, have led to activated carbons with surface area as
255 high as 2000 m^2 g^{-1} [49].

256 The impregnation with H_2SO_4 has been demonstrated to develop porosity, but to a
257 lesser extent if compared to KOH [50]; however, it modifies the surface groups,
258 promoting the appearance of carboxylic groups [51] to the detriment of hydroxyl and
259 carbonyl groups observed in the activation with KOH [52,53]. From the characterization
260 results of **Table 2**, it can be observed that the textural modifications with H_2SO_4 are

marginal, with a slight increase in the surface area and total pore volume but negligible microporosity.

Table 2. Textural characterization of the activated chars

Sample	S_{BET} (m^2 g^{-1})	S_{MP} (m^2 g^{-1})	V_T (cm^3 g^{-1})	V_{MP} (cm^3 g^{-1})	V_{MP}/V_T (%)
P-char	33	15	0.042	<0.001	-
80P-char	6	< 0.1	0.017	<0.001	-
50P-char	5	< 0.1	0.008	<0.001	-
20P-char	< 0.1	< 0.1	<0.001	<0.001	-
OS-char	< 0.1	< 0.1	<0.001	<0.001	-
P-char-KOH	508	401	0.403	0.204	50.6
80P-char-KOH	559	472	0.343	0.231	67.3
50P-char-KOH	380	340	0.216	0.168	77.7
20P-char-KOH	280	251	0.164	0.131	79.9
OS-char-KOH	194	172	0.116	0.089	76.7
P-char-H_2SO_4	36	< 0.1	0.084	<0.001	-
80P-char- H_2SO_4	14	< 0.1	0.038	<0.001	-
50P-char- H_2SO_4	3.4	< 0.1	0.017	<0.001	-
20P-char- H_2SO_4	0.6	< 0.1	0.004	<0.001	-
OS-char- H_2SO_4	0.4	< 0.1	0.002	<0.001	-

*S_{BET}: total specific surface area by BET method; S_{MP}: micropore surface area; V_T: total pore volume; V_{MP}: micropore volume.

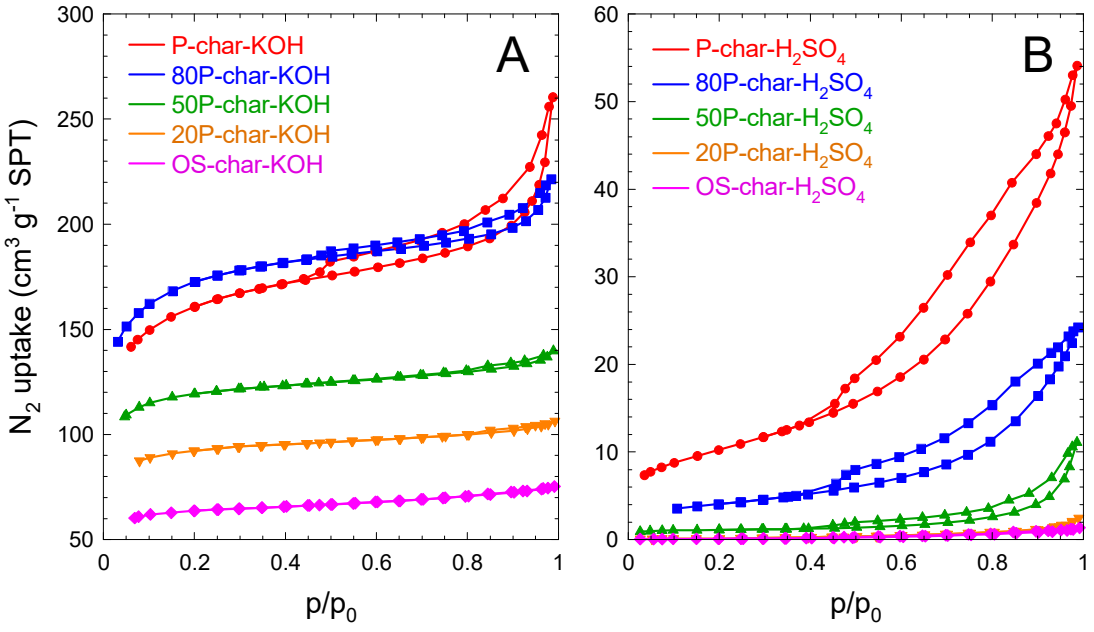

Figure 1. N_2 adsorption-desorption isotherms of the chars activated with KOH (A) and H_2SO_4 (B).

XRD was conducted to characterize the disorder degree of carbon and level of crystallization of the chars after activation, see the diffractograms of some selected samples activated with KOH in **Figure 2**. The broad bands centered at approximately 24 and 43°, corresponding respectively to the (002) and (100) diffraction planes, were observed in the samples [54]. The broadness of the peaks is a clear indication of the great degree of disorder. The band observed in the samples at the (002) plane can be related to a small number of stacked layers with a uniform interlayer distance (3.7 Å), a value larger than the usually reported for ordered structures based on graphite or graphene [55]. **Figure 2** also depicts the presence of a minor contribution of other crystalline phases, probably due to the presence of metallic impurities. Although an attempt was conducted, the complexity of the samples, the low intensity of these peaks, and the plausible interaction with the carbon phase at the high temperatures during activation [54] did not enable a clear identification.

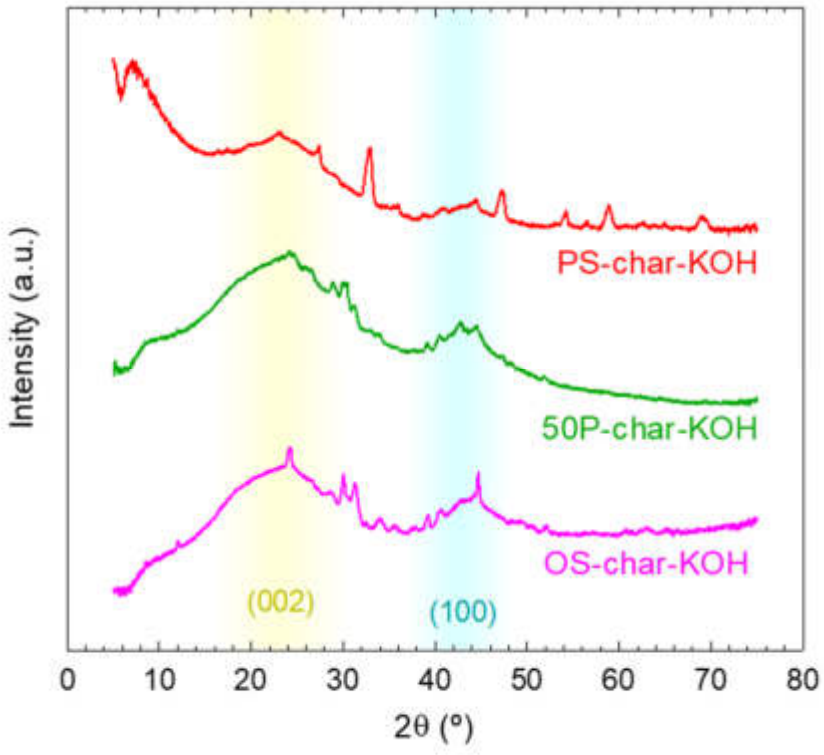

Figure 2. XRD patterns of the chars activated with KOH

The nature of the functional groups present in the samples was studied by FTIR analysis. **Figure 3** depicts the FTIR spectra of the non-activated char and char activated with H_2SO_4 and KOH obtained from the plastic and olive stone precursors as a selection to depict the differences between the precursor's nature. The mixtures led to intermediate FTIR footprints depending on the contribution of plastic or olive stone to the char. The same functional groups were observed either in plastic or olive stone chars without activation with slight differences. A wide band centered at around 3100 cm^{-1} is observed in both chars, slightly higher in the char prepared from the plastic. At 1600 cm^{-1}, a peak is associated with C=C stretching in aromatic rings [56,57]. At 1400 cm^{-1} is defined as another peak that can be attributed to medium vibration of O-H flexion in carboxylic acids, alcohol, or phenol. At 1200 cm^{-1}, another peak belonging to C-O vibration in carboxylic acids [57,58]. At 1100 cm^{-1} there is another peak attributable to C-O of ether or alcohols [57,59]. The olive stone char displayed a uniform contribution of the abovementioned peaks whereas the plastic char if compared in intensity, was characterized by the higher contribution of alkenes and ethers and/or alcohols. After activation, more remarkable differences were observed between the nature of the chemical agent, e.g. KOH and H_2SO_4. The activation with KOH decreased the intensity of ethers and alcohols. Nonetheless, the use of H_2SO_4 contributed to obtaining oxygenated peaks with more intensity than the use of KOH. This tendency, although common in both precursors, is more visible in the case of plastic char.

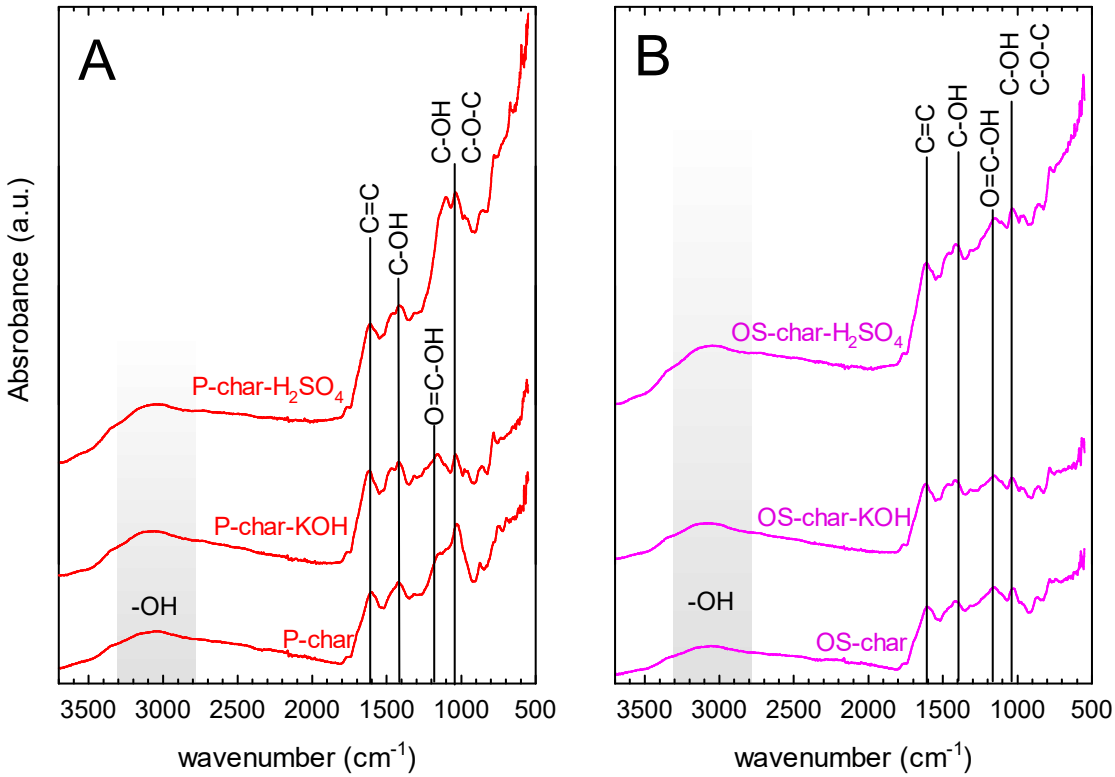

Figure 3. FTIR spectra of plastic (A) and olive stone (B) chars before and after activation with KOH and H_2SO_4.

The elemental composition of the activated chars is shown in **Table 3**. The activated char prepared from olive contains a considerably higher amount of carbon and less oxygen than the material prepared with plastic. The activation of the chars with KOH led to a decrease in these differences in carbon content, being the material prepared from olive stone slightly enriched in carbon if compared to the plastic one. The reaction between the KOH and the oxygenated content present in the plastic char to release CO_2 may explain the increase of carbon content and enhance the formation of cavities that contribute to the microporosity of the material [60]. On the contrary, the activation with H_2SO_4 promoted the carbon content differences between the plastic and olive stone chars. During the activation process, not only does the carbon react with sulfuric acid to release CO_2 and SO_2, but also oxygen is fixed onto the surface as

318 oxygenated groups that contribute to the percentual account of oxygen. This effect of an
319 increase in the oxygen proportion during H_2SO_4 activation compared to KOH has been
320 also reported during the activation of tires [61]. Moreover, the presence of sulfur was
321 detected, at a higher proportion as the content of plastic in the precursor char was
322 higher, probably due to the higher reaction extent between the char and the acid,
323 triggering the release of larger amounts of sulfate [61].

324 **Table 3.** Elemental composition of the chars before and after activation

Material	Composition (%)				
	N	C	H	S	O
P-char	0.48	55.03	2.75	0.05	41.69
80P-char	n.d.	65.03	2.07	n.d.	32.90
50P-char	n.d.	70.91	3.12	n.d.	25.97
20P-char	n.d.	78.41	3.44	0.04	18.11
OS-char	n.d.	83.07	3.52	n.d.	13.41
P-char-KOH	0.64	75.83	0.77	n.d.	22.76
80P-char-KOH	0.63	75.56	0.74	n.d.	23.07
50P-char-KOH	0.68	75.83	0.71	n.d.	22.78
20P-char-KOH	0.35	76.54	0.69	n.d.	22.42
OS-char-KOH	0.00	78.59	0.63	n.d.	20.78
P-char-H_2SO_4	n.d.	40.52	0.76	5.19	53.53
80P-char- H_2SO_4	0.21	44.35	1.74	3.89	49.81
50P-char- H_2SO_4	n.d.	55.97	0.36	4.88	38.79
20P-char- H_2SO_4	0.68	62.69	0.75	0.33	35.55
OS-char- H_2SO_4	0.72	75.12	0.86	0.19	23.11

325 n.d.: not detected

326 The morphology of the activated carbons was analyzed by SEM technique. **Figure 4**
327 illustrates some of the selected SEM micrographs obtained for the activated chars with
328 KOH, which developed the highest microporosity. The sample obtained from the olive
329 stones, OS-char-KOH (**Figures 4A and 4B**), displayed holey particles. The images
330 obtained with the polystyrene precursor, P-char-KOH, provided a completely different
331 morphology. It was observed that the agglomeration of fiber particles, see **Figure 4C**.
332 The magnification over these fibers suggested the presence of some cavities (**Figure**

4D). The samples obtained from the mixture of both precursors led to heterogeneous contributions of the previously mentioned morphologies, i.e. holy particles to which fibers were attached. **Figures 4E and 4F** provide the view of the holey particles of 50P-char-KOH.

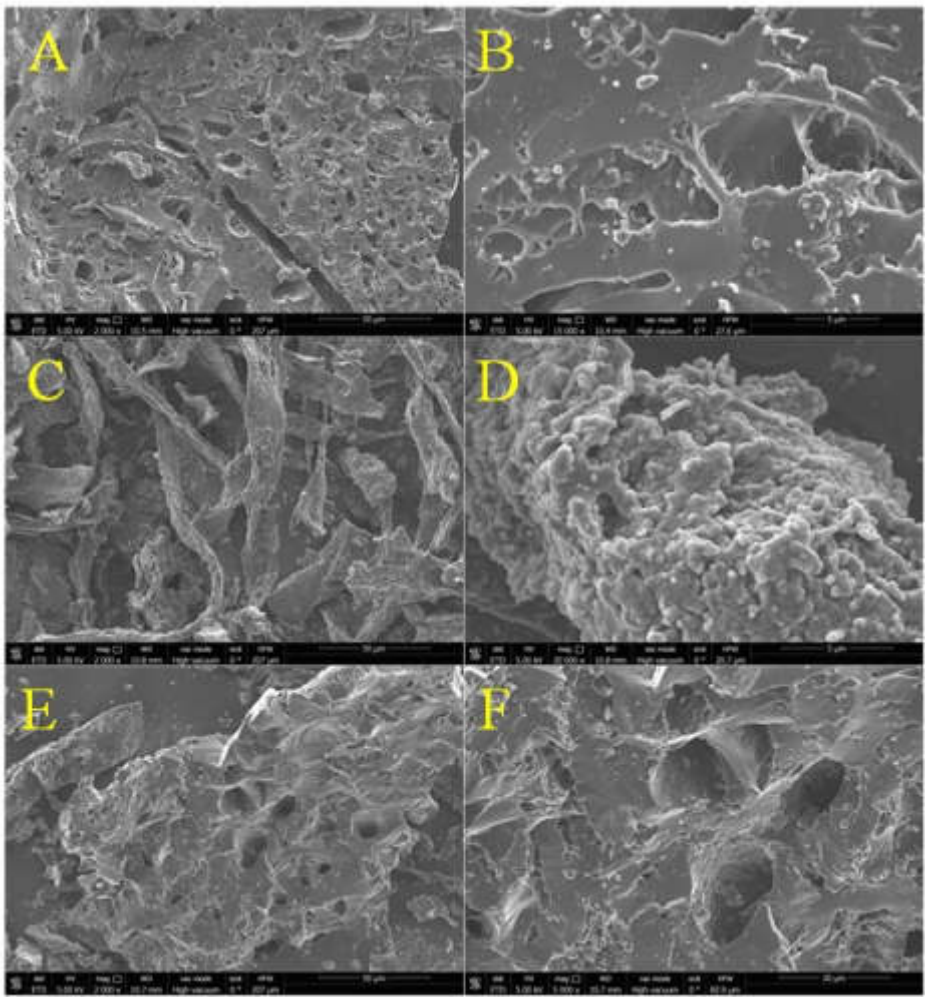

Figure 4. SEM pictures of OS-char-KOH (A and B), P-char-KOH (C and D), and 50P-char-KOH (E and F).

The morphology at a higher magnification than SEM was evaluated by TEM microscopy. The P-char-KOH and OS-char-KOH were selected for the TEM analysis, see **Figure 5**. In the selected pictures taken, it is observed that the particles of P-char-KOH displayed higher thickness, leading to particles opaque to TEM. In contrast, OS-char-KOH was much more transparent, depicting wrapped carbon plates and fibers, agglomerated in higher units of particles. The recorded EEL spectra of P-char-KOH and

OS-char-KOH, see Figure 5D and 5H respectively display the peaks of π* (286 eV) and σ* (293 eV) transitions, of the carbon-K core-loss edge. These spectra provide information on the disorder degree of carbon in each sample. The feature at 286 eV, linked to the transition 1s→π* is attributed to the C=C double bonds; while the acquired peak defined at 291 eV, corresponding to the transition 1s→σ* is attributed to C-C bonds of characteristic of diamond and graphitic structures [62]. In ordered compounds like diamond and graphite, a peak appears at 291 eV [63]. Moreover, while the intensity gradually decreases with the energy loss in amorphous carbon, the graphitic structure describes a wide second peak within 320 and 330 eV [63], as shown in the sample P-char-KOH. Accordingly, the EELS analysis of P-char-KOH can be labeled as graphitic whereas the OS-char-KOH displays EELS carbon-K spectra of an amorphous structure. It should be mentioned that the spectrum of P-char-KOH was defined with low intensity due to the thickness and opaqueness of the sample, impeding a high flow of transmitted electrons.

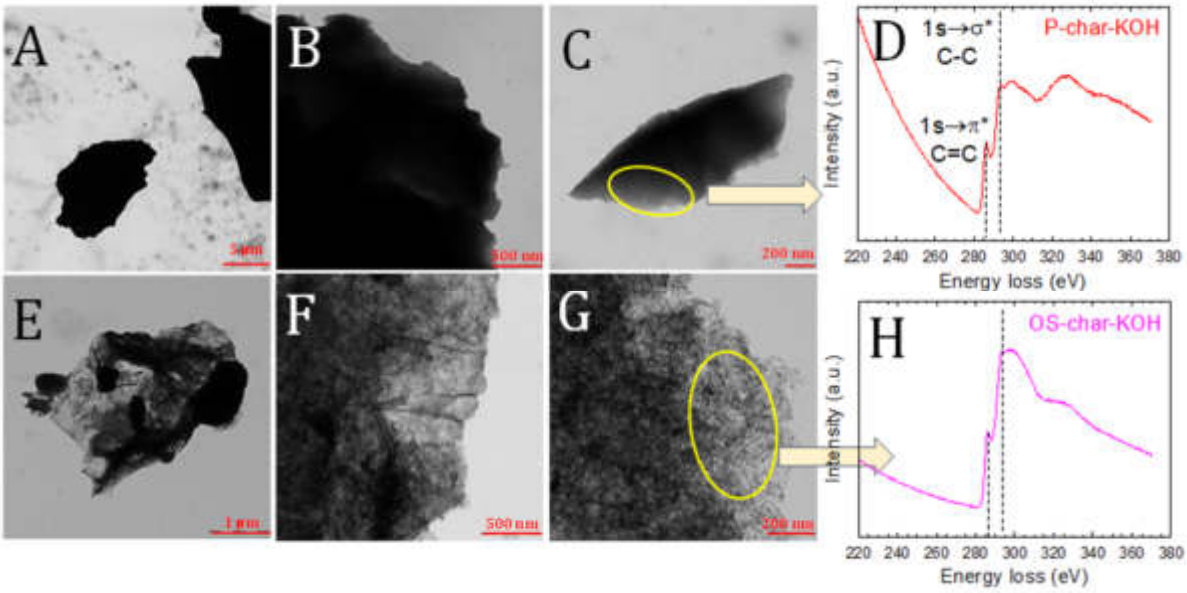

Figure 5. TEM pictures and EELS analysis of the carbon-K core-loss edge of P-char-KOH (A- D) and OS-char-KOH (E-H).

363 ### 3.2. Adsorption of CO_2 by thermogravimetry

364 The activated chars were tested as adsorbent for CO_2 capture. As a first approach to
365 determine the adsorption capacity, the performance on thermobalance with a pure CO_2
366 effluent was tested. The temporal evolution of the retained CO_2 is depicted in **Figure 6**
367 and the saturation CO_2 capacity, quantified from the reached plateau, is illustrated in
368 **Figure 7**. The chars before activation displayed low adsorption capacity, being the char
369 obtained from olive stones was more effective than the plastic, i.e. 43.7 vs 31.3 mg g^{-1}.
370 The char prepared with the mixtures of plastic and olive stone led to intermediated
371 values. After the washing with HCl, these values were slightly decreased, being 41.6 mg
372 g^{-1} for the olive stone and 29.1 mg g^{-1} for the washed plastic char. The activation with
373 KOH was more efficient than H_2SO_4 for the capture of CO_2 by adsorption.

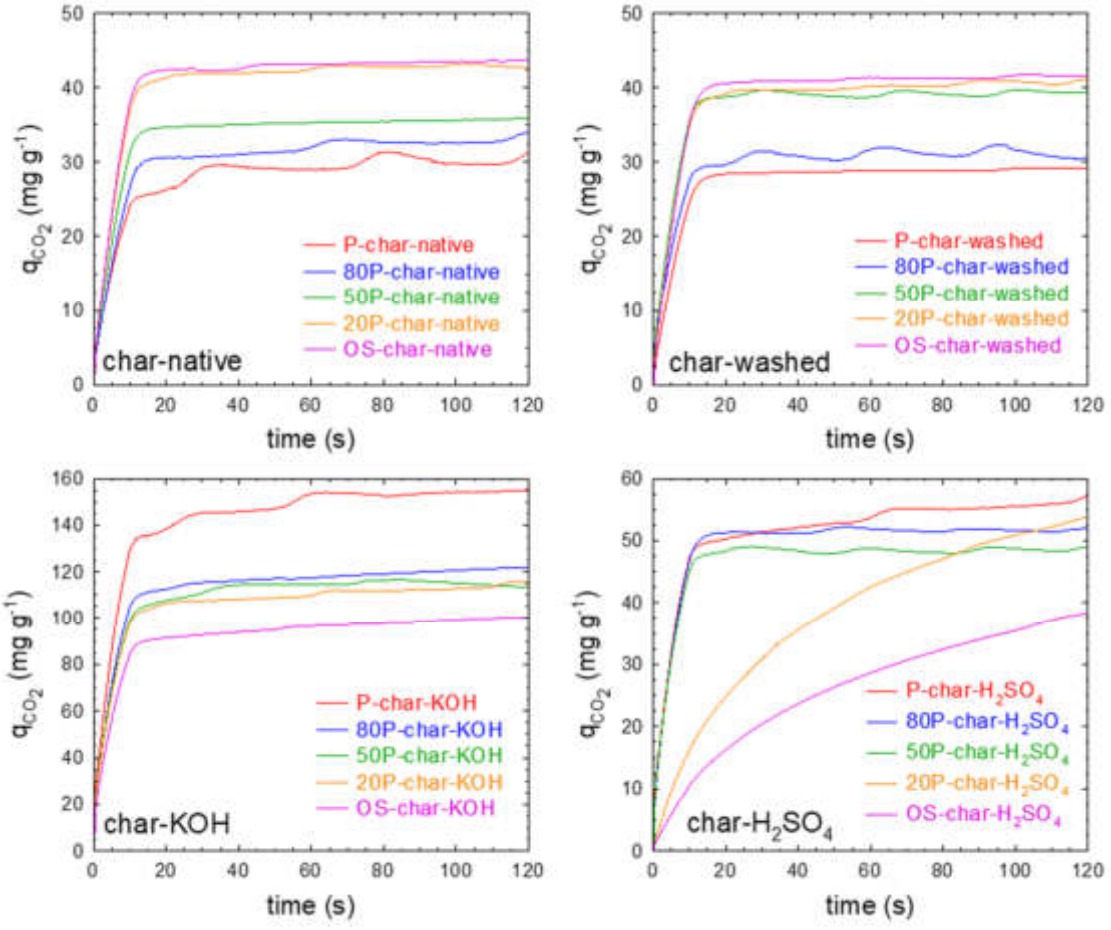

374
375 **Figure 6**. CO_2 adsorption performance on thermobalance of the materials before and
376 after activation

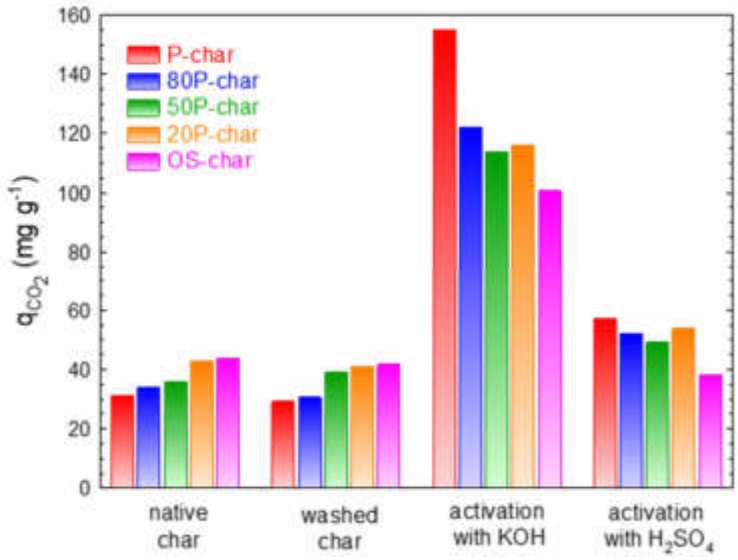

Figure 7. Comparison of the saturation CO_2 capacities with the different materials

Contrary to what was registered with the char before activation, the P-char after activation produced better adsorption of CO_2. For instance, the P-char-KOH was able to retain 155 mg CO_2 g^{-1} whereas the OS-char-KOH adsorbed a third less, 100.3 mg CO_2 g^{-1}. This improved adsorption capacity can be explained based on the textural properties, i.e. micropore volume 0.204 cm^3 g^{-1} (P-char-KOH) vs 0.089 cm^3 g^{-1} (OS-char-KOH). It is frequently reported a proportional relationship between the amount of adsorbed CO_2 and the micropore volume (< 2 nm) [64,65]. The CO_2 molecule displays a diameter of 0.33 nm, and slightly higher sizes but inferior to 1 nm result in the optimum value for CO_2 adsorption [66]. The pore size distribution was studied through CO_2 adsorption isotherm at 0 ºC. **Figure 8** depicts the results of the pore width distribution by the HK model, in which it can be appreciated that the micropore of the char after activation is within 0.5 and 2.5 nm, being the most frequent ~0.6 nm. The activation with KOH was able to develop an important contribution to microporosity, which has been reported as essential for CO_2 capture. Although the intermediate mixtures did not display a synergistic effect on the CO_2 adsorption, their combination can be justified based on the higher yield of material they produce after pyrolysis as

shown in **Table 1**. The addition of plastic as raw material aided not only in developing a higher microporosity but also in enhancing the CO_2 adsorption capacity. The literature reports diverse CO_2 uptakes depending on the microporosity developed.

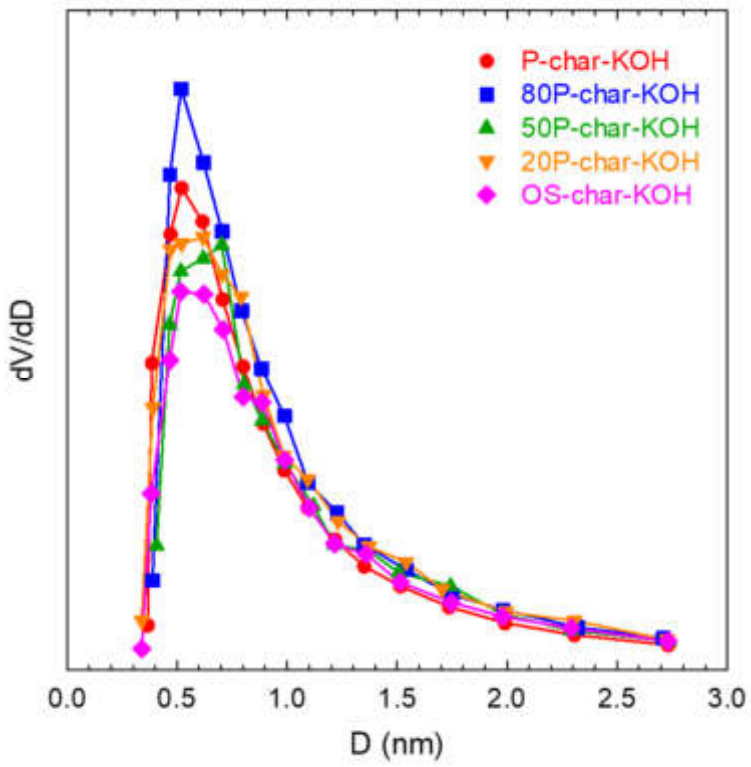

Figure 8. Micropore size distribution of the samples activated with KOH by the HK method.

The use of plastic polymers has been considered as a carbon source precursor for the activation for the production of porous activated carbon which can be used for the adsorption of CO_2. Nonetheless, there is little information in the literature using polystyrene as the precursor. There is a work that reported the preparation of carbonaceous materials with steam activation and superficial tunning with nitrogen-enriched groups, able to uptake CO_2 with a performance of 140.8 mg g^{-1} [67]. For the comparison with the material prepared in this work, e.g. from polystyrene, the closest polymer with wide study in the literature is polyethylene terephthalate (PET). For instance, the activation of the char obtained from post-consumer PET soft-drink bottles with KOH (500 ºC, KOH ratio 4:1) led to a CO_2 uptake of 96.8 mg g^{-1} [68]. PET from

411 disposable water and cold drink bottles has been also used to prepare activated carbon
412 (KOH, 700 ºC, ratio 3:1), leading to a retention of 101.6 mg g^{-1} [69]. Under activation
413 conditions closer to our study (activation with KOH, 800 ºC, ratio 1:1), the adsorption
414 capacity has been reported as high as 154 mg g^{-1} [70], quite close to the value reached in
415 this work (155 mg g^{-1}). The olive stones have been used to obtain competitive materials
416 for CO_2 adsorption but with lower capacities than polymers. For example, the olive
417 stones carbonized and activated with CO_2 have been reported to uptake at atmospheric
418 pressure 88 mg g^{-1} [71].

419 The activation with H_2SO_4 poorly improved the results obtained with the chars
420 before activation, see **Figure 7**. Only a slight improvement was observed, especially
421 when plastic is present in the mixture of the precursor char. For example, the P-char-
422 H_2SO_4 adsorbed 57.3 mg g^{-1}. In the case of OS-char-H_2SO_4, the value was 38.3 mg g^{-1},
423 even lower than before the activation. This behavior can be related to the textural
424 porosity. The addition of H_2SO_4 poorly developed porosity in the precursor chars, with
425 negligible microporosity contribution, explains the lack of CO_2 adsorption ability. For
426 this reason, the H_2SO_4 was discharged as an activation method in this study. Other
427 works have successfully got activation with H_2SO_4 although reaching less porosity
428 compared to KOH. The activation of date seeds with H_2SO_4 led to surface areas 311-
429 577 m^2 g^{-1} while KOH raised the values to 623-912 m^2 g^{-1}, depending on the chemical
430 activating ratio and temperature [72]. However, although KOH led to the highest
431 porosity, it was H_2SO_4 that conducted the best CO_2 uptake in comparison due to the
432 presence of surface acid groups.

433 The kinetics of CO_2 adsorption onto carbonaceous materials have been fitted to
434 diverse models, e.g. Lagergren's pseudo-first order, Ho's pseudo-second order, or
435 Elovich's diffusional model [28,35]. The pseudo-first order model assumes reversible

436 interaction between the adsorbent and the adsorbate, such as physisorption. The pseudo-
437 second order supposes a strong binding interaction between the adsorbed gas and the
438 surface of the solid, which is appropriate to describe chemisorption processes [73]. The
439 CO_2 adsorption onto activated carbon has been largely described as a physisorption
440 process [34], as the reported adsorption heat suggests [34,74,75]. Based on this premise,
441 the adsorption kinetics has been examined by fitting to the pseudo-first order and the
442 Avrami model, a factorial variant of the pseudo-first order with three parameters.
443 Although the pseudo-second order and Elovich models have been adjusted to the
444 experimental data (results not shown), the lack of adequate fitting (R^2<0.9 in most of
445 the cases) if compared to the pseudo-first order (R^2>0.9) suggests a probable
446 physisorption predominant action. The results of the obtained fittings are shown in
447 **Table 4**. The Avrami model implies a better description, raising in all the cases the R^2
448 values. In general terms, the rate constant, either k_1 or k_A, displayed minor differences
449 between the samples. The adsorption rate onto the native chars was improved as the
450 olive stone proportion was raised and even improved with the washing step. The
451 activated samples with KOH performed similar rate constants to their washed ones. The
452 k-values of the activated samples are within the typical values reported in the literature
453 for activated carbons, i.e. 0.18-0.30 min^{-1} [76,77]. The activation of H_2SO_4 slightly
454 raised the k-values except for the samples with the highest proportion of olive stone, in
455 which the kinetic was dramatically decreased, probably due to the lack of enough
456 developed porosity, as the S_{BET} inferior to 1 m^2 g^{-1} suggests.

Table 4. Kinetics parameters of CO_2 adsorption on the materials before and after activation with KOH and H_2SO_4

Sample	$q_{120\ min}$ (mg g^{-1})	Pseudo-first order			Avrami			
		$q_{CO_2} = q_S(1 - e^{-k_1 t})$			$q_{CO_2} = q_S(1 - e^{-(k_A t)^{n_A}})$			
		q_S (mg g^{-1})	k_1 (min^{-1})	R^2	q_S (mg g^{-1})	k_A (min^{-1})	n_A	R^2
P-char-native	31.3	29.7	0.144	0.965	29.9	0.147	0.799	0.987
80P-char-native	34.0	32.2	0.156	0.972	32.2	0.156	1.080	0.986
50P-char-native	35.6	35.5	0.180	0.987	35.4	0.174	1.213	0.994
20P-char-native	42.6	42.7	0.171	0.989	42.6	0.167	1.192	0.993
OS-char-native	43.7	43.3	0.177	0.986	43.2	0.111	1.243	0.993
P-char-washed	29.1	29.0	0.164	0.985	28.9	0.158	1.305	0.996
80P-char-washed	30.6	31.1	0.188	0.981	31.1	0.189	0.987	0.990
50P-char-washed	39.2	39.3	0.195	0.987	39.3	0.188	1.187	0.992
20P-char-washed	41.1	40.4	0.168	0.987	40.3	0.164	1.216	0.993
OS-char-washed	41.6	41.4	0.164	0.985	41.3	0.158	1.305	0.996
P-char-KOH	155.1	150.9	0.170	0.969	152.2	0.173	0.771	0.978
80P-char-KOH	122.0	118.4	0.194	0.981	118.7	0.198	0.887	0.991
50P-char-KOH	113.7	114.3	0.189	0.981	114.9	0.196	0.803	0.990
20P-char-KOH	115.9	110.9	0.196	0.974	111.3	0.201	0.850	0.989
OS-char-KOH	100.5	96.9	0.184	0.970	97.3	0.188	0.837	0.974
P-char-H_2SO_4	57.3	54.1	0.181	0.955	54.6	0.184	0.747	0.965
80P-char-H_2SO_4	52.0	51.8	0.205	0.991	51.7	0.201	1.099	0.993
50P-char-H_2SO_4	49.0	48.6	0.221	0.989	48.6	0.218	1.068	0.990
20P-char-H_2SO_4	53.8	53.4	0.028	0.990	62.9	0.019	0.751	0.999
OS-char-H_2SO_4	38.3	38.7	0.024	0.988	51.3	0.013	0.719	0.999

The thermodynamic behavior of the adsorption process was studied by carrying out CO_2 adsorption isotherms up to atmospheric pressure at 0 ºC and 25 ºC for the samples activated with KOH due to the higher adsorption uptakes, as suggested by the assays carried out in the thermobalance. The shape of the isotherms, see **Figure 9A**, depicts a growing rise of the CO_2 uptake until 101 kPa, with the lack of a defined plateau. The exothermic behavior of the adsorption process was confirmed by the decrease of CO_2 uptake with the rise of the temperature. The experimental data were successfully adjusted to the Freundlich equation (R^2>0.99), see the results in **Table 5**. The Freundlich equation is an empirical model that describes a non-ideal and reversible

process of monolayer or multilayer adsorption on a heterogeneous surface [27]. Therefore, the good fitting to the Freundlich isotherm suggests certain heterogeneity in the activated carbon surface [78]. The Freundlich constant (K_F) decreased with the temperature, due to the physisorption character; and the exponent was higher than the unit, which is characteristic of a physisorption process [79]. If the samples are compared, the chars prepared from the mixture of plastic and olive stone show certain improvement in CO_2 uptake if compared to the original precursors.

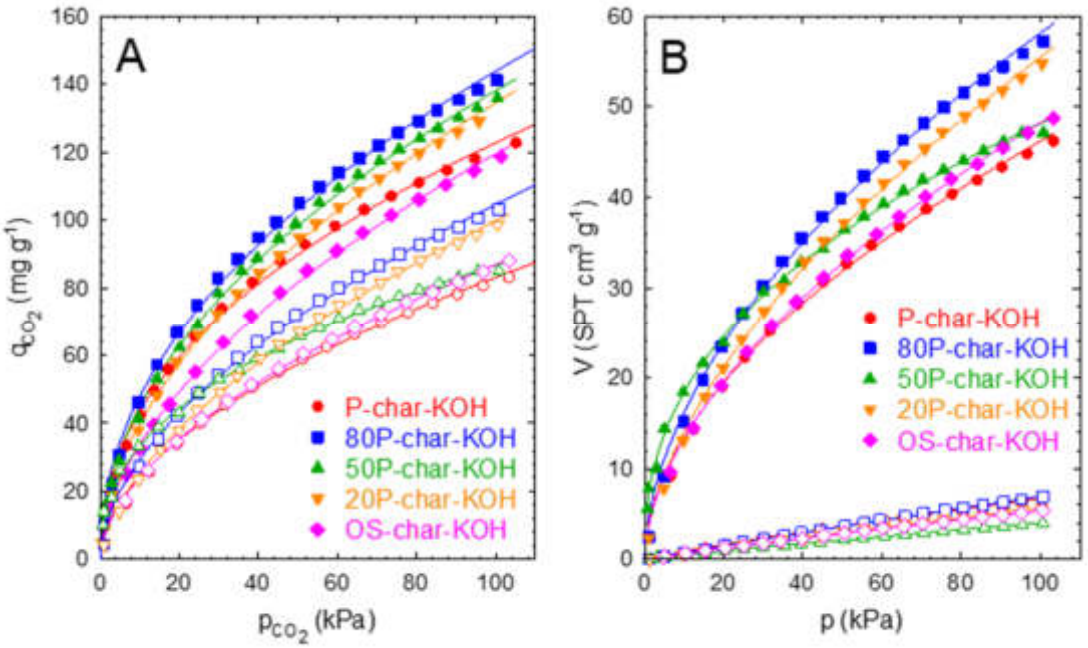

Figure 9. (A) CO_2 adsorbed (mg g^{-1}) at 0 ºC (filled symbols) and 25 ºC (empty symbols). (B) CO_2 (filled symbols) and N_2 (empty symbols) gas uptake (SPT cm^3 g^{-1}) at 25 ºC. The lines depict the fitting to the Freundlich model.

Table 5 Freundlich parameters of CO_2 adsorption, CO_2/N_2 selectivity at 25 ºC, and isosteric adsorption heat.

Sample	T (ºC)	Freundlich isotherm $q_{CO_2} = K_F\, p^{1/n_F}$			q_{CO2} (mg g^{-1}) at 1 bar	CO_2/N_2 Selectivity[2] (%)		$-\Delta H_{ads}$[3] (kJ mol^{-1})
		K_F[1]	n_F	R^2		initial	$IAST_{15:85}$	
P-char-KOH	0	15.395	2.214	0.996	123.8	10.2	39.0	23.9
	25	7.068	1.868	0.997	84.6			
80P-char-KOH	0	15.902	2.091	0.997	144.5	14.1	47.3	20.1
	25	8.195	1.808	0.997	105.2			

50P-char-KOH	0	14.520	2.045	0.998	138.0	17.3	68.3	28.2
	25	7.068	1.868	0.997	83.2			
20P-char-KOH	0	11.837	1.894	0.998	135.4	15.4	55.1	16.6
	25	6.428	1.679	0.998	100.4			
OS-char-KOH	0	9.845	1.817	0.996	124.8	12.6	50.8	21.7
	25	6.068	1.787	0.999	80.3			

[1] K_F in mg g^{-1} kPa^{-nF}

[2] Initial selectivity obtained at 25 ºC from the slopes of CO_2 and N_2 isotherms. $IAST_{15:85}$, selectivity obtained for a CO_2:N_2 mixture of 15:85 (v/v) at ambient pressure.

[3] Isosteric adsorption heat at q_{CO2}= 80 mg g^{-1}.

The CO_2/N_2 selectivity of the activated samples with KOH was assessed following two approaches. Firstly, the initial selectivity, e.g. the selectivity at low pressures with equal partial pressures of CO_2 and N_2, was calculated as the division of the slope of the straight line adjusted to the isotherms illustrated in **Figure 9B** at low pressures (0-20 kPa), leading to the values displayed in **Table 5**. Alternatively, the selectivity was also estimated from the ideal adsorbed solution theory (IAST), see **Figure 10A**, as a function of the pressure for a hypothetical mixture of 15:85 CO_2:N_2, a value frequently observed in exhausted fumes released from fuel combustion. Both calculations for the selectivity lead to the same conclusion, the selectivity of the samples prepared from mixed precursors was higher than those activated with the pure chars of olive stone or plastic. Furthermore, the sample 50-char-KOH shows an outstanding synergistic effect in terms of selectivity as visible in **Figure 10A**. At ambient pressure, this sample displayed an IAST selectivity of 68.3, higher than the values reported for commercial formulas of activated carbons (<15) [30] and quite competitive to the majority of experimental carbon materials prepared at lab scale [80], which provides evidence of the benefits of mixing char precursors for CO_2-capture and separation applications.

The isosteric heat of CO_2 adsorption of the chars activated with KOH is depicted in **Figure 10B**. It is observed that the samples containing polystyrene as a precursor led to profiles in which the isosteric heat of adsorption was larger at low coverage uptake and

gradually declined with the consumption of strong active sites. This behavior is attributed to the heterogeneity of the sample in which the first active sites led to higher exothermicity than the rest. The equation of Freundlich assumes that the adsorption energy logarithmically decreases with the number of available adsorption sites decreases [78]. At atmospheric pressure, the obtained values are within 16-38 kJ mol^{-1}. Values below 40 kJ mol^{-1} are considered as physisorption, whereas values over 80 kJ mol^{-1} are labeled as chemisorption [81]. As suggested by the calculated Freundlich exponents values, the CO_2 process on the prepared samples takes place via physisorption.

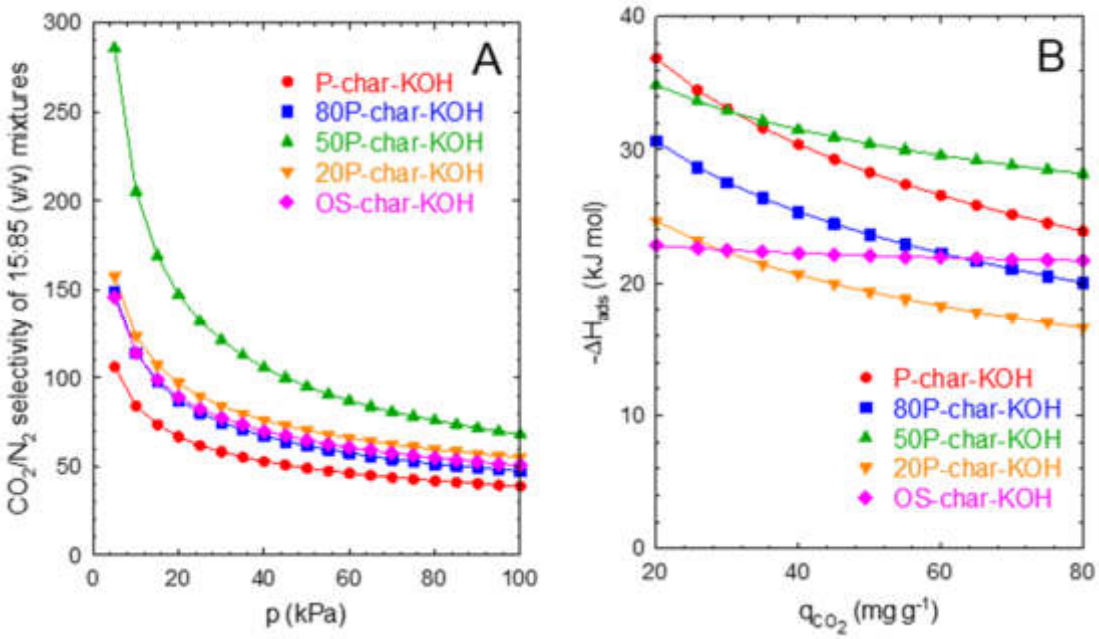

Figure 8. (A) IAST CO_2/N_2 selectivity at 25 ºC of 15:85 (v/v) mixtures and isosteric heat of CO_2 adsorption of the samples activated with KOH as a function of the pressure.

3.3. Breakthrough curves of CO_2 adsorption

The dynamic behavior of CO_2 adsorption was assessed in the fixed-bed column for the chars activated with KOH based on the better results achieved in the thermobalance assays. **Figure 11** illustrates the breakthrough curves of the chars activated with KOH which led to the best adsorption capacities. Three inlet CO_2 concentrations within 10-

30% vol. were tested. The higher the inlet concentration of CO_2, the faster the breakthrough curve was described. At the lowest inlet CO_2, the curves showed the highest differences among them. Under a feeding of 10% of CO_2 the sample activated from pure plastic pyrolysis led, i.e. P-char-KOH, led the breakthrough curve appeared at 46 s, with an adsorption capacity of q_{CO2}=49.7 mg g^{-1}. The adsorbent prepared from olive stone (OS-char-KOH) shortened the appearance of the breakthrough point (~36 s) and retained less CO_2, q_{CO2}=47.8 mg g^{-1}. The sample whose char was obtained from 80% of plastic, i.e. 80P-char-KOH led to the highest adsorption capacity, q_{CO2}=59.6 mg g^{-1}. The rest of the samples, see **Table 6**, reported very similar adsorption retention if compared to the sample with only olive stone. Regarding the removal percentages of CO_2, the sample P-char-KOH led to the best results and the OS-char-KOH to the lowest efficiency, with intermediate values for the mixtures.

An increase in the inlet CO_2 concentration gave a rise in the adsorption capacities, for instance in the case of P-char-KOH, the adsorption capacities increased to 176.3 mg g^{-1} at 30% and 220.8 mg g^{-1} at 50%. At the same time, the saturation times were shortened. This positive effect is associated with the larger probability of the adsorbate molecules interacting with the active points of the adsorbent. Besides, with an increase in CO_2 concentration, a greater concentration gradient is generated; therefore, the resistance mass transfer is reduced, leading to a greater adsorption capacity [82,83]. The adsorption capacities obtained with the different plastic-olive stone mass ratios at 30 and 50% of CO_2 feeding led to similar behavior if compared to those obtained at 10% of CO_2. Thus, the P-char-KOH conducted the highest CO_2 adsorption capacity followed by 80P-char-KOH and OS-char-KOH. The other two intermediate proportions, i.e. 50P-char-KOH and 20P-char-KOH produced slightly lower retention capacities.

Table 6. Adsorption capacities and removal efficiency of CO_2 during the sequential adsorption-desorption cycles in the fixed-bed column at different initial concentrations

Sample	C_0=10%		C_0=30%		C_0=50%	
	q_{CO2} (mg g^{-1})	R (%)	q_{CO2} (mg g^{-1})	R (%)	q_{CO2} (mg g^{-1})	R (%)
P-char-KOH	49.7	34.8	176.3	33.6	220.8	32.8
80P-char-KOH	59.6	36.2	172.9	31.9	216.4	35.4
50P-char-KOH	49.5	38.5	137.7	40.5	190.1	33.9
20P-char-KOH	50.2	31.3	152.3	31.8	197.7	31.4
OS-char-KOH	47.8	29.7	161.3	28.7	197.5	27.5

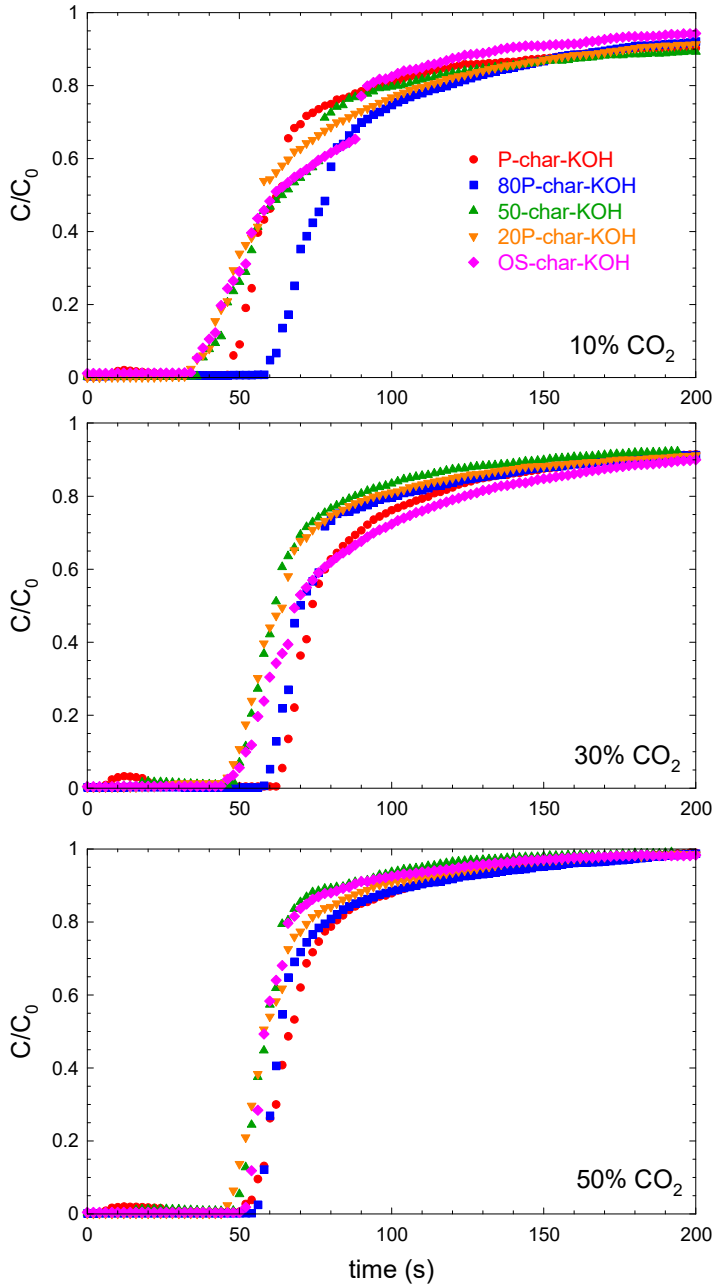

Figure 11. Breakthrough curves at different inlet concentrations of CO_2 of the chars activated with KOH. Experimental conditions: T=30 ºC, m_{Ads}=0.5 g, υ_{GAS}=100 mL min^{-1}.

If the retention capacities obtained in the fixed-bed column are compared to the saturation capacities obtained in the thermobalance assays, it is observed that the values obtained in the column are higher. This might be attributed to the humidity present in the sample when carrying out the column experiments. The thermobalance analysis program includes a step at 200 ºC which was not carried out in the fixed bed column. The presence of moisture has been linked to higher CO_2 uptake due to the reaction of CO_2 and water to release carbonate and bicarbonate, increasing therefore the amount of CO_2 consumed. For example, in the case of modified commercial silica, an increase of up to 10% of CO_2 adsorbed has been reported in the presence of humidity [84]. Not only has the moisture been highlighted as the reason why the fixed-bed experiments display higher saturation uptakes, but also the operating conditions. The adsorbent particles in the thermobalance, placed in a capsule, are likely to build aggregates that impede the adsorbate from reaching internal pores, making the material impermeable to the adsorbate molecules [85]. On the contrary, the fluid-dynamic conditions displayed in the fixed bed help to maximize the surface exposed to the adsorbate and avoid the formation of aggregates.

To further investigate the dynamic behavior of the samples, adsorption-desorption cycles of CO_2 were carried out. As an example, the two different materials prepared from polystyrene or olive stone, i.e. the samples P-char-KOH and OS-char-KOH, were selected. The low partial pressure of CO_2 and 30 ºC were selected in an attempt to simulate post-combustion conditions. **Figure 12** depicts the evolution of three consecutive adsorption and desorption cycles. The capacity of CO_2 retention during the adsorption step and the release in the desorption step are shown in **Table 7**. As observed from the adsorption capacities, no loss of retention was registered on the materials. The desorbed amount of CO_2 calculated from the desorption curves was slightly inferior to

576 the estimated for the adsorption step, i.e. in the case of P-char-KOH the adsorbed
577 capacity was 145-155 mg g^{-1}, and the desorbed 111-125 mg g^{-1}.

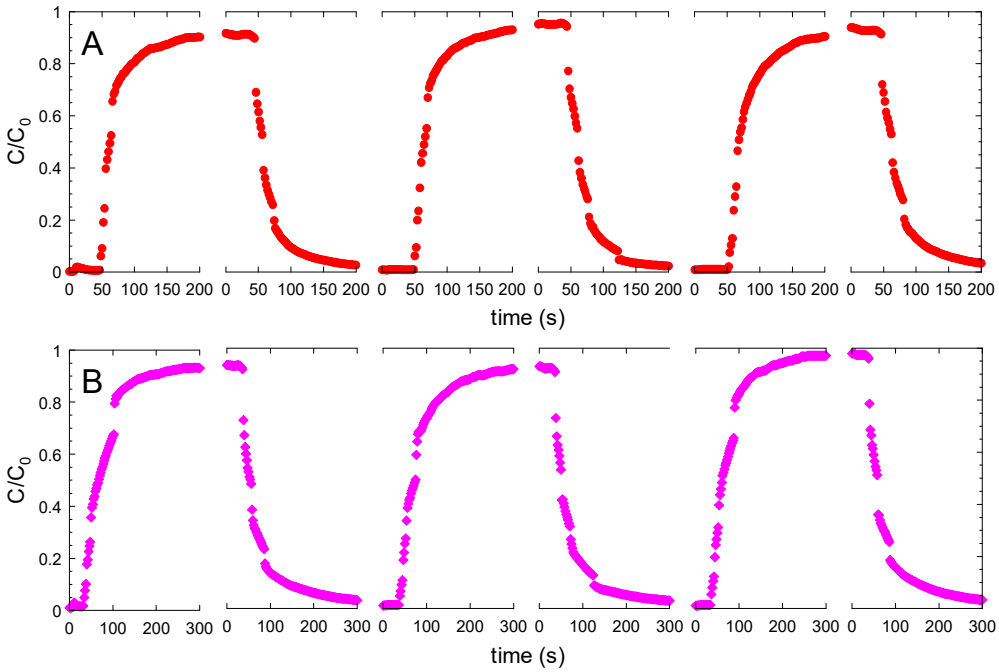

578
579 **Figure 12.** Breakthrough curves of sequential adsorption-desorption cycles of CO_2 with
580 P-char-KOH (A) and OS-char-KOH (B). Experimental conditions: T=30 ºC, m_{Ads}=0.5
581 g, υ_{GAS}=100 mL min^{-1}, C_0=30%.

582 **Table 7.** Adsorption capacities (mg g^{-1}) of CO_2 during the sequential adsorption-
583 desorption cycles in the fixed-bed column

Cycle	Step	P-char-KOH	OS-char-KOH
1	Adsorption	49.7	47.8
	Desorption	37.1	38.0
2	Adsorption	48.3	50.4
	Desorption	40.1	37.6
3	Adsorption	51.8	44.9
	Desorption	41.7	41.2

584 **4. CONCLUSIONS**

585 Plastic residues and olive stone can be easily transformed into added-value activated
586 carbon with a high ability to capture CO_2 in gas streams. The pyrolysis of olive stones
587 leads to a higher char yield than polystyrene. The activation with KOH resulted in more
588 effective than the impregnation with H_2SO_4. The activation with KOH was able to boost

589 surface areas as high as 504 and 194 m^2 g^{-1} for polystyrene and olive stone chars,
590 respectively; while H_2SO_4 barely raised the porosity of the starting materials. The
591 performance of CO_2 adsorption in thermobalance assays was conducted to the best
592 results for those materials prepared with KOH, with a good correlation between the CO_2
593 uptake and the microporosity developed. The KOH activation of the char from plastic
594 led to a 155 mg CO_2 g^{-1} uptake, while olive stone led to 100 mg CO_2 g^{-1}. Activation
595 with H_2SO_4 enhanced the adsorption capability of the non-activated char but to a much
596 lesser extent than KOH. Adsorption assays in a fixed-bed column were performed at
597 different CO_2 inlet concentrations (10-50%), having a positive influence on the
598 saturation CO_2 uptake. The capacity of the plastic char activated with KOH was similar
599 to the achieved with olive stone, and higher than the values obtained with
600 thermobalance analysis at 50% CO_2 feeding, probably due to the better contact of the
601 adsorbate and the adsorbent in the column. Finally, sequential adsorption-desorption
602 cycles were carried out in the column, showing a lack of loss in the adsorption retention.
603 This work suggests the possibility of mixing plastic and biomass residues to enhance the
604 yield in the preparation of the material with no loss of CO_2 performance.

605 **Acknowledgments**

606 This work belongs to the project PDC2022-133808-I00, funded by
607 MCIN/AEI/10.13039/501100011033 and the European Union "NextGeneration
608 EU"/PRTR. The authors thank the support provided by the external services of the
609 University of Granada (“Centro de Instrumentación Científica”, CIC) for the help with
610 the characterization of the samples.

611

References

[1] J. McGlade, I. Samy Fahim, D. Green, P. Landrigan, A. Andrady, M. Costa, R. Geyer, R. Gomes, A. Tan Shau Hwai, J. Jambeck, D. Li, C. Rochman, P. Ryan, M. Thiel, R. Thompson, K. Townsend, A. Turra, From Pollution To Solution: a global assessment of marine litter and plastic pollution, 2021. https://nottingham-repository.worktribe.com/output/8047115 (accessed April 29, 2023).

[2] B.C. Gibb, Plastics are forever, Nature Chemistry 2019 11:5. 11 (2019) 394–395. https://doi.org/10.1038/s41557-019-0260-7.

[3] A. Hasan Anik, S. Hossain, M. Alam, M. Binte Sultan, M.T. Hasnine, M.M. Rahman, Microplastics pollution: A comprehensive review on the sources, fates, effects, and potential remediation, Environ Nanotechnol Monit Manag. 16 (2021) 100530. https://doi.org/10.1016/J.ENMM.2021.100530.

[4] V. Godoy, M.A. Martín-Lara, M. Calero, G. Blázquez, Physical-chemical characterization of microplastics present in some exfoliating products from Spain, Mar Pollut Bull. 139 (2019) 91–99. https://doi.org/10.1016/J.MARPOLBUL.2018.12.026.

[5] X.Z. Lim, Microplastics are everywhere - but are they harmful?, Nature. 593 (2021) 22–25. https://doi.org/10.1038/D41586-021-01143-3.

[6] A.M. Amadei, E. Sanyé-Mengual, S. Sala, Modeling the EU plastic footprint: Exploring data sources and littering potential, Resour Conserv Recycl. 178 (2022) 106086. https://doi.org/10.1016/J.RESCONREC.2021.106086.

[7] T. Thiounn, R.C. Smith, Advances and approaches for chemical recycling of plastic waste, Journal of Polymer Science. 58 (2020) 1347–1364. https://doi.org/10.1002/POL.20190261.

[8] A. Lee, M.S. Liew, Tertiary recycling of plastics waste: an analysis of feedstock, chemical and biological degradation methods, J Mater Cycles Waste Manag. 23 (2021) 32–43. https://doi.org/10.1007/S10163-020-01106-2.

[9] B. Zhu, D. Wang, N. Wei, Enzyme discovery and engineering for sustainable plastic recycling, Trends Biotechnol. 40 (2022) 22–37. https://doi.org/10.1016/J.TIBTECH.2021.02.008.

[10] M.S. Qureshi, A. Oasmaa, H. Pihkola, I. Deviatkin, A. Tenhunen, J. Mannila, H. Minkkinen, M. Pohjakallio, J. Laine-Ylijoki, Pyrolysis of plastic waste: Opportunities and challenges, J Anal Appl Pyrolysis. 152 (2020) 104804. https://doi.org/10.1016/J.JAAP.2020.104804.

[11] T. Maqsood, J. Dai, Y. Zhang, M. Guang, B. Li, Pyrolysis of plastic species: A review of resources and products, J Anal Appl Pyrolysis. 159 (2021) 105295. https://doi.org/10.1016/J.JAAP.2021.105295.

[12] M. Calero, R.R. Solís, M.J. Muñoz-Batista, A. Pérez, G. Blázquez, M. Ángeles Martín-Lara, Oil and gas production from the pyrolytic transformation of

651 recycled plastic waste: An integral study by polymer families, Chem Eng Sci.
652 271 (2023) 118569. https://doi.org/10.1016/J.CES.2023.118569.

653 [13] D.A. Wijesekara, P. Sargent, C.J. Ennis, D. Hughes, Prospects of using chars
654 derived from mixed post waste plastic pyrolysis in civil engineering applications,
655 J Clean Prod. 317 (2021) 128212.
656 https://doi.org/10.1016/J.JCLEPRO.2021.128212.

657 [14] C. Abdy, Y. Zhang, J. Wang, Y. Yang, I. Artamendi, B. Allen, Pyrolysis of
658 polyolefin plastic waste and potential applications in asphalt road construction: A
659 technical review, Resour Conserv Recycl. 180 (2022) 106213.
660 https://doi.org/10.1016/J.RESCONREC.2022.106213.

661 [15] J. Jamradloedluk, C. Lertsatitthanakorn, Characterization and Utilization of Char
662 Derived from Fast Pyrolysis of Plastic Wastes, Procedia Eng. 69 (2014) 1437–
663 1442. https://doi.org/10.1016/J.PROENG.2014.03.139.

664 [16] M. Sogancioglu, E. Yel, G. Ahmetli, Pyrolysis of waste high density
665 polyethylene (HDPE) and low density polyethylene (LDPE) plastics and
666 production of epoxy composites with their pyrolysis chars, J Clean Prod. 165
667 (2017) 369–381. https://doi.org/10.1016/J.JCLEPRO.2017.07.157.

668 [17] M. Sogancioglu, A. Yucel, E. Yel, G. Ahmetli, Production of Epoxy Composite
669 from the Pyrolysis Char of Washed PET Wastes, Energy Procedia. 118 (2017)
670 216–220. https://doi.org/10.1016/J.EGYPRO.2017.07.022.

671 [18] S. Kumar, E. Singh, R. Mishra, A. Kumar, S. Caucci, Utilization of Plastic
672 Wastes for Sustainable Environmental Management: A Review, ChemSusChem.
673 14 (2021) 3985–4006. https://doi.org/10.1002/CSSC.202101631.

674 [19] R. Acosta, V. Fierro, A. Martinez de Yuso, D. Nabarlatz, A. Celzard,
675 Tetracycline adsorption onto activated carbons produced by KOH activation of
676 tyre pyrolysis char, Chemosphere. 149 (2016) 168–176.
677 https://doi.org/10.1016/J.CHEMOSPHERE.2016.01.093.

678 [20] R.R. Solís, M.Á. Martín-Lara, A. Ligero, J. Balbís, G. Blázquez, M. Calero,
679 Revalorizing a Pyrolytic Char Residue from Post-Consumer Plastics into
680 Activated Carbon for the Adsorption of Lead in Water, Applied Sciences. 12
681 (2022) 8032. https://doi.org/10.3390/APP12168032/S1.

682 [21] F. Hussin, M.K. Aroua, M.A. Kassim, U. Fazara, M. Ali, C.: Hussin, F.; Aroua,
683 M.K.; Kassim, M.A.; Ali, Transforming Plastic Waste into Porous Carbon for
684 Capturing Carbon Dioxide: A Review, Energies (Basel). 14 (2021) 8421.
685 https://doi.org/10.3390/EN14248421.

686 [22] S. Pérez-Huertas, M. Calero, A. Ligero, A. Pérez, K. Terpiłowski, M.A. Martín-
687 Lara, On the use of plastic precursors for preparation of activated carbons and
688 their evaluation in CO_2 capture for biogas upgrading: a review, Waste
689 Management. 161 (2023) 116–141.
690 https://doi.org/10.1016/J.WASMAN.2023.02.022.

[23] A. Ligero, M. Calero, M.Á. Martín-Lara, G. Blázquez, R.R. Solís, A. Pérez, Fixed-bed CO_2 adsorption onto activated char from the pyrolysis of a non-recyclable plastic mixture from real urban residues, Journal of CO_2 Utilization. 73 (2023) 102517. https://doi.org/10.1016/J.JCOU.2023.102517.

[24] A. Ligero, M. Calero, A. Pérez, R.R. Solís, M.J. Muñoz-Batista, M.Á. Martín-Lara, Low-cost activated carbon from the pyrolysis of post-consumer plastic waste and the application in CO_2 capture, Process Safety and Environmental Protection. 173 (2023) 558–566. https://doi.org/10.1016/J.PSEP.2023.03.041.

[25] P.A. Gauden, A.P. Terzyk, G. Rychlicki, P. Kowalczyk, M.S. Ćwiertnia, J.K. Garbacz, Estimating the pore size distribution of activated carbons from adsorption data of different adsorbates by various methods, J Colloid Interface Sci. 273 (2004) 39–63. https://doi.org/10.1016/J.JCIS.2003.08.033.

[26] R.J. Dombrowski, C.M. Lastoskie, D.R. Hyduke, The Horvath–Kawazoe method revisited, Colloids Surf A Physicochem Eng Asp. 187–188 (2001) 23–39. https://doi.org/10.1016/S0927-7757(01)00618-5.

[27] H. Freundlich, Über die Adsorption in Lösungen, Zeitschrift Für Physikalische Chemie. 57U (1907) 385–470. https://doi.org/10.1515/ZPCH-1907-5723.

[28] S. Wang, Y.R. Lee, Y. Won, H. Kim, S.E. Jeong, B. Wook Hwang, A. Ra Cho, J.Y. Kim, Y. Cheol Park, H. Nam, D.H. Lee, H. Kim, S.H. Jo, Development of high-performance adsorbent using KOH-impregnated rice husk-based activated carbon for indoor CO_2 adsorption, Chemical Engineering Journal. 437 (2022) 135378. https://doi.org/10.1016/J.CEJ.2022.135378.

[29] Y. Liao, J. Weber, C.F.J. Faul, Fluorescent microporous polyimides based on perylene and triazine for highly CO_2-selective carbon materials, Macromolecules. 48 (2015) 2064–2073. https://doi.org/10.1021/MA501662R.

[30] H. Li, J. Li, A. Thomas, Y. Liao, Ultra-High Surface Area Nitrogen-Doped Carbon Aerogels Derived From a Schiff-Base Porous Organic Polymer Aerogel for CO_2 Storage and Supercapacitors, Adv Funct Mater. 29 (2019) 1904785. https://doi.org/10.1002/ADFM.201904785.

[31] A. Nuhnen, C. Janiak, A practical guide to calculate the isosteric heat/enthalpy of adsorption via adsorption isotherms in metal–organic frameworks, MOFs, Dalton Transactions. 49 (2020) 10295–10307. https://doi.org/10.1039/D0DT01784A.

[32] S. He, G. Chen, H. Xiao, G. Shi, C. Ruan, Y. Ma, H. Dai, B. Yuan, X. Chen, X. Yang, Facile preparation of N-doped activated carbon produced from rice husk for CO_2 capture, J Colloid Interface Sci. 582 (2021) 90–101. https://doi.org/10.1016/J.JCIS.2020.08.021.

[33] M.S. Shafeeyan, W.M.A.W. Daud, A. Shamiri, N. Aghamohammadi, Modeling of Carbon Dioxide Adsorption onto Ammonia-Modified Activated Carbon: Kinetic Analysis and Breakthrough Behavior, Energy and Fuels. 29 (2015) 6565–6577. https://doi.org/10.1021/ACS.ENERGYFUELS.5B00653.

731 [34] P. Ammendola, F. Raganati, R. Chirone, CO_2 adsorption on a fine activated
732 carbon in a sound assisted fluidized bed: Thermodynamics and kinetics,
733 Chemical Engineering Journal. 322 (2017) 302–313.
734 https://doi.org/10.1016/J.CEJ.2017.04.037.

735 [35] L. Stevens, K. Williams, W.Y. Han, T. Drage, C. Snape, J. Wood, J. Wang,
736 Preparation and CO_2 adsorption of diamine modified montmorillonite via
737 exfoliation grafting route, Chemical Engineering Journal. 215–216 (2013) 699–
738 708. https://doi.org/10.1016/J.CEJ.2012.11.058.

739 [36] N. Díez, P. Álvarez, M. Granda, C. Blanco, R. Santamaría, R. Menéndez, CO_2
740 adsorption capacity and kinetics in nitrogen-enriched activated carbon fibers
741 prepared by different methods, Chemical Engineering Journal. 281 (2015) 704–
742 712. https://doi.org/10.1016/J.CEJ.2015.06.126.

743 [37] M. Avrami, Kinetics of Phase Change. I General Theory, J Chem Phys. 7 (1939)
744 1103–1112. https://doi.org/10.1063/1.1750380.

745 [38] R. Serna-Guerrero, A. Sayari, Modeling adsorption of CO_2 on amine-
746 functionalized mesoporous silica. 2: Kinetics and breakthrough curves, Chemical
747 Engineering Journal. 161 (2010) 182–190.
748 https://doi.org/10.1016/J.CEJ.2010.04.042.

749 [39] M. Songolzadeh, M. Soleimani, M. Takht Ravanchi, Using modified Avrami
750 kinetic and two component isotherm equation for modeling of CO_2/N_2 adsorption
751 over a 13X zeolite bed, J Nat Gas Sci Eng. 27 (2015) 831–841.
752 https://doi.org/10.1016/J.JNGSE.2015.09.029.

753 [40] J.B. Condon, An Overview of Physisorption, in: Surface Area and Porosity
754 Determinations by Physisorptiontion, Elsevier Science, 2006: pp. 1–27.
755 https://doi.org/10.1016/B978-044451964-1/50003-0.

756 [41] M. Thommes, Physical Adsorption Characterization of Nanoporous Materials,
757 Chemie Ingenieur Technik. 82 (2010) 1059–1073.
758 https://doi.org/10.1002/CITE.201000064.

759 [42] F.G.F. de Paula, M.C.M. de Castro, P.F.R. Ortega, C. Blanco, R.L. Lavall, R.
760 Santamaría, High value activated carbons from waste polystyrene foams,
761 Microporous and Mesoporous Materials. 267 (2018) 181–184.
762 https://doi.org/10.1016/J.MICROMESO.2018.03.027.

763 [43] H. Teng, Y.C. Lin, L.Y. Hsu, Production of Activated Carbons from Pyrolysis of
764 Waste Tires Impregnated with Potassium Hydroxide, J Air Waste Manage Assoc.
765 50 (2011) 1940–1946. https://doi.org/10.1080/10473289.2000.10464221.

766 [44] R. Acosta, D. Nabarlatz, A. Sánchez-Sánchez, J. Jagiello, P. Gadonneix, A.
767 Celzard, V. Fierro, Adsorption of Bisphenol A on KOH-activated tyre pyrolysis
768 char, J Environ Chem Eng. 6 (2018) 823–833.
769 https://doi.org/10.1016/J.JECE.2018.01.002.

770 [45] A. Boonpoke, S. Meesiri, N. Seayang, W. Homnan, Polyethylene terephthalate
771 based activated carbon production: preliminary study on KOH activation with

772 microwave assist, GEOMATE Journal. 19 (2020) 17–24.
773 https://doi.org/10.21660/2020.76.4579.

774 [46] R.R. Solís, M.Á. Martín-Lara, A. Ligero, J. Balbís, G. Blázquez, M. Calero,
775 Revalorizing a Pyrolytic Char Residue from Post-Consumer Plastics into
776 Activated Carbon for the Adsorption of Lead in Water, Applied Sciences. 12
777 (2022) 8032. https://doi.org/10.3390/APP12168032.

778 [47] R. Ubago-Pérez, F. Carrasco-Marín, D. Fairén-Jiménez, C. Moreno-Castilla,
779 Granular and monolithic activated carbons from KOH-activation of olive stones,
780 Microporous and Mesoporous Materials. 92 (2006) 64–70.
781 https://doi.org/10.1016/J.MICROMESO.2006.01.002.

782 [48] T.M. Alslaibi, I. Abustan, M.A. Ahmad, A. Abu Foul, Preparation of Activated
783 Carbon From Olive Stone Waste: Optimization Study on the Removal of Cu^{2+},
784 Cd^{2+}, Ni^{2+}, Pb^{2+}, Fe^{2+}, and Zn^{2+} from Aqueous Solution Using Response Surface
785 Methodology, J Dispers Sci Technol. 35 (2014) 913–925.
786 https://doi.org/10.1080/01932691.2013.809506.

787 [49] E.; Diaz, I.; Sanchis, C.J.; Coronella, A.F. Mohedano, E. Diaz, I. Sanchis, C.J.
788 Coronella, A.F. Mohedano, Activated Carbons from Hydrothermal Carbonization
789 and Chemical Activation of Olive Stones: Application in Sulfamethoxazole
790 Adsorption, Resources. 11 (2022) 43.
791 https://doi.org/10.3390/RESOURCES11050043.

792 [50] F.J. Sánchez-Borrego, T.J. Barea de Hoyos-Limón, J.F. García-Martín, P.
793 Álvarez-Mateos, Production of Bio-Oils and Biochars from Olive Stones:
794 Application of Biochars to the Esterification of Oleic Acid, Plants. 11 (2021) 70.
795 https://doi.org/10.3390/PLANTS11010070.

796 [51] G. Cimino, R.M. Cappello, C. Caristi, G. Toscano, Characterization of carbons
797 from olive cake by sorption of wastewater pollutants, Chemosphere. 61 (2005)
798 947–955. https://doi.org/10.1016/J.CHEMOSPHERE.2005.03.042.

799 [52] S.J. Park, W.Y. Jung, Effect of KOH activation on the formation of oxygen
800 structure in activated carbons synthesized from polymeric precursor, J Colloid
801 Interface Sci. 250 (2002) 93–98. https://doi.org/10.1006/JCIS.2002.8309.

802 [53] Z. Lendzion-Bieluń, Czekajło, D. Sibera, D. Moszyński, J. Sreńscek-Nazzal,
803 A.W. Morawski, R.J. Wrobel, B. Michalkiewicz, W. Arabczyk, U. Narkiewicz,
804 Surface characteristics of KOH-treated commercial carbons applied for CO_2
805 adsorption, Adsorption Science and Technology. 36 (2018) 478–492.
806 https://doi.org/10.1177/0263617417704527.

807 [54] J. Bedia, M. Peñas-Garzón, A. Gómez-Avilés, J.J. Rodriguez, C. Belver, Review
808 on Activated Carbons by Chemical Activation with $FeCl_3$, C Journal of Carbon
809 Research. 6 (2020) 21. https://doi.org/10.3390/C6020021.

810 [55] Z.Q. Li, C.J. Lu, Z.P. Xia, Y. Zhou, Z. Luo, X-ray diffraction patterns of graphite
811 and turbostratic carbon, Carbon N Y. 45 (2007) 1686–1695.
812 https://doi.org/10.1016/J.CARBON.2007.03.038.

[56] A.P. Terzyk, The influence of activated carbon surface chemical composition on the adsorption of acetaminophen (paracetamol) in vitro: Part II. TG, FTIR, and XPS analysis of carbons and the temperature dependence of adsorption kinetics at the neutral pH, Colloids Surf A Physicochem Eng Asp. 177 (2001) 23–45. https://doi.org/10.1016/S0927-7757(00)00594-X.

[57] J. Yang, K.Q. Qiu, Preparation of Activated Carbon by Chemical Activation under Vacuum, Environ Sci Technol. 43 (2009) 3385–3390. https://doi.org/10.1021/ES8036115.

[58] S. Shin, J. Jang, S.H. Yoon, I. Mochida, A study on the effect of heat treatment on functional groups of pitch based activated carbon fiber using FTIR, Carbon N Y. 35 (1997) 1739–1743. https://doi.org/10.1016/S0008-6223(97)00132-2.

[59] S.M. Yakout, G. Sharaf El-Deen, Characterization of activated carbon prepared by phosphoric acid activation of olive stones, Arabian Journal of Chemistry. 9 (2016) S1155–S1162. https://doi.org/10.1016/J.ARABJC.2011.12.002.

[60] M. Hu, Z. Ye, Q. Zhang, Q. Xue, Z. Li, J. Wang, Z. Pan, Towards understanding the chemical reactions between KOH and oxygen-containing groups during KOH-catalyzed pyrolysis of biomass, Energy. 245 (2022) 123286. https://doi.org/10.1016/J.ENERGY.2022.123286.

[61] R.B. González-González, L.T. González, S. Iglesias-González, E. González-González, S.O. Martinez-Chapa, M. Madou, M.M. Alvarez, A. Mendoza, Characterization of Chemically Activated Pyrolytic Carbon Black Derived from Waste Tires as a Candidate for Nanomaterial Precursor, Nanomaterials. 10 (2020) 2213. https://doi.org/10.3390/NANO10112213.

[62] P.G. González, Y.B. Pliego-Cuervo, Physicochemical and microtextural characterization of activated carbons produced from water steam activation of three bamboo species, J Anal Appl Pyrolysis. 99 (2013) 32–39. https://doi.org/10.1016/J.JAAP.2012.11.004.

[63] V. Jeanne-Rose, V. Golabkan, J.L. Mansot, L. Largitte, T. Césaire, A. Ouensanga, An EELS-based study of the effects of pyrolysis on natural carbonaceous materials used for activated charcoal preparation, J Microsc. 210 (2003) 53–59. https://doi.org/10.1046/J.1365-2818.2003.01170.X.

[64] S.M. Hong, E. Jang, A.D. Dysart, V.G. Pol, K.B. Lee, CO_2 Capture in the Sustainable Wheat-Derived Activated Microporous Carbon Compartments, Scientific Reports 2016 6:1. 6 (2016) 1–10. https://doi.org/10.1038/srep34590.

[65] S. Acevedo, L. Giraldo, J.C. Moreno-Piraján, Adsorption of CO_2 on Activated Carbons Prepared by Chemical Activation with Cupric Nitrate, ACS Omega. 5 (2020) 10423–10432. https://doi.org/10.1021/ACSOMEGA.0C00342.

[66] T. Guo, W. Tian, Y. Wang, Effect of Pore Structure on CO_2 Adsorption Performance for $ZnCl_2$/$FeCl_3$/H_2O(g) Co-Activated Walnut Shell-Based Biochar, Atmosphere (Basel). 13 (2022) 1110. https://doi.org/10.3390/ATMOS13071110/S1.

[67] X. Ren, C. Zhang, L. Kou, R. Wang, Y. Wang, R. Li, Hierarchical porous polystyrene-based activated carbon spheres for CO_2 capture, Environmental Science and Pollution Research. 29 (2022) 13098–13113. https://doi.org/10.1007/S11356-021-16561-Z.

[68] A. Arenillas, F. Rubiera, J.B. Parra, C.O. Ania, J.J. Pis, Surface modification of low cost carbons for their application in the environmental protection, Appl Surf Sci. 252 (2005) 619–624. https://doi.org/10.1016/J.APSUSC.2005.02.076.

[69] B. Kaur, J. Singh, R.K. Gupta, H. Bhunia, Porous carbons derived from polyethylene terephthalate (PET) waste for CO_2 capture studies, J Environ Manage. 242 (2019) 68–80. https://doi.org/10.1016/J.JENVMAN.2019.04.077.

[70] M. Adibfar, T. Kaghazchi, N. Asasian, M. Soleimani, Conversion of poly(ethylene terephthalate) waste into activated carbon: chemical activation and characterization, Chem Eng Technol. 37 (2014) 979–986. https://doi.org/10.1002/CEAT.201200719.

[71] M. Puig-Gamero, A. Esteban-Arranz, L. Sanchez-Silva, P. Sanchez, Obtaining activated biochar from olive stone using a bench scale high-pressure thermobalance, J Environ Chem Eng. 9 (2021) 105374. https://doi.org/10.1016/J.JECE.2021.105374.

[72] A.E. Ogungbenro, D. V. Quang, K.A. Al-Ali, L.F. Vega, M.R.M. Abu-Zahra, Synthesis and characterization of activated carbon from biomass date seeds for carbon dioxide adsorption, J Environ Chem Eng. 8 (2020) 104257. https://doi.org/10.1016/J.JECE.2020.104257.

[73] V.K. Singh, E.A. Kumar, Comparative Studies on CO_2 Adsorption Kinetics by Solid Adsorbents, Energy Procedia. 90 (2016) 316–325. https://doi.org/10.1016/J.EGYPRO.2016.11.199.

[74] J. Singh, S. Basu, H. Bhunia, Dynamic CO_2 adsorption on activated carbon adsorbents synthesized from polyacrylonitrile (PAN): Kinetic and isotherm studies, Microporous and Mesoporous Materials. 280 (2019) 357–366. https://doi.org/10.1016/J.MICROMESO.2019.02.031.

[75] J. Singh, H. Bhunia, S. Basu, Adsorption of CO_2 on KOH activated carbon adsorbents: Effect of different mass ratios, J Environ Manage. 250 (2019) 109457. https://doi.org/10.1016/J.JENVMAN.2019.109457.

[76] M. Wei, Q. Yu, H. Xie, Z. Zuo, L. Hou, F. Yang, Kinetics studies of CO_2 adsorption and desorption on waste ion-exchange resin-based activated carbon, Int J Hydrogen Energy. 42 (2017) 27122–27129. https://doi.org/10.1016/J.IJHYDENE.2017.09.102.

[77] A.L. Yaumi, M.Z.A. Bakar, B.H. Hameed, Melamine-nitrogenated mesoporous activated carbon derived from rice husk for carbon dioxide adsorption in fixed-bed, Energy. 155 (2018) 46–55. https://doi.org/10.1016/J.ENERGY.2018.04.183.

[78] J. Serafin, B. Dziejarski, Application of isotherms models and error functions in activated carbon CO_2 sorption processes, Microporous and Mesoporous

Materials. 354 (2023) 112513. https://doi.org/10.1016/J.MICROMESO.2023.112513.

[79] F. Haghseresht, G.Q. Lu, Adsorption Characteristics of Phenolic Compounds onto Coal-Reject-Derived Adsorbents, Energy and Fuels. 12 (1998) 1100–1107. https://doi.org/10.1021/EF9801165.

[80] M. Oschatz, M. Antonietti, A search for selectivity to enable CO_2 capture with porous adsorbents, Energy Environ Sci. 11 (2018) 57–70. https://doi.org/10.1039/C7EE02110K.

[81] T.A. Saleh, Adsorption technology and surface science, Interface Science and Technology. 34 (2022) 39–64. https://doi.org/10.1016/B978-0-12-849876-7.00006-3.

[82] Y.L. Tan, M.A. Islam, M. Asif, B.H. Hameed, Adsorption of carbon dioxide by sodium hydroxide-modified granular coconut shell activated carbon in a fixed bed, Energy. 77 (2014) 926–931. https://doi.org/10.1016/J.ENERGY.2014.09.079.

[83] R.J. Hook, An Investigation of Some Sterically Hindered Amines as Potential Carbon Dioxide Scrubbing Compounds, Ind Eng Chem Res. 36 (1997) 1779–1790. https://doi.org/10.1021/IE9605589.

[84] E.S. Sanz-Pérez, M. Olivares-Marín, A. Arencibia, R. Sanz, G. Calleja, M.M. Maroto-Valer, CO_2 adsorption performance of amino-functionalized SBA-15 under post-combustion conditions, International Journal of Greenhouse Gas Control. 17 (2013) 366–375. https://doi.org/10.1016/J.IJGGC.2013.05.011.

[85] F. Raganati, P. Ammendola, R. Chirone, CO_2 adsorption on fine activated carbon in a sound assisted fluidized bed: Effect of sound intensity and frequency, CO_2 partial pressure and fluidization velocity, Appl Energy. 113 (2014) 1269–1282. https://doi.org/10.1016/J.APENERGY.2013.08.073.